

Chlorine oxidation of VOCs at a semi-rural site in Beijing: Significant chlorine liberation from ClNO₂ and subsequent gas and particle phase Cl-VOC production

Michael Le Breton¹, Åsa M Hallquist², Ravi Kant Pathak¹, David Simpson^{3,4}, Yujue Wang⁵, John Johansson³, Jing Zheng⁵, Yudong Yang⁵, Dongjie Shang⁵, Haichao Wang⁵, Qianyun Liu⁶, Chak Chan⁷, Tao Wang⁸, Thomas J. Bannan⁹, Michael Priestley⁹, Carl J. Percival^{9*}, Dudley E. Shallcross^{10,11}, Keding Lu⁵, Song Guo⁵, Min Hu⁵ and Mattias Hallquist¹

¹Department of Chemistry and Molecular Biology, University of Gothenburg, Gothenburg, Sweden

²IVL Swedish Environmental Research Institute, Gothenburg, Sweden

³Earth and Space Sciences, Chalmers University of Technology, Gothenburg, Sweden

⁴Norwegian Meteorological Institute, Oslo, Norway

⁵State Key Joint Laboratory of Environmental Simulation and Pollution Control, College of Environmental Sciences and Engineering, Peking University, Beijing, China

⁶Division of Environment and Sustainability, The Hong Kong University of Science and Technology, Clearwater Bay, Kowloon, Hong Kong

⁷School of Energy and Environment, City University of Hong Kong, Hong Kong

⁸Department of Civil and Environmental Engineering, The Hong Kong Polytechnic University, Hong Kong, China

⁹Centre for Atmospheric Science, School of Earth, Atmospheric and Environmental Science, University of Manchester, Manchester, UK

¹⁰School of Chemistry, University of Bristol, Cantock's Close, Bristol, BS8 1TS, UK

¹¹[Department of Chemistry, University of the Western Cape, Bellville, Cape Town, South Africa.](#)

* Now at Jet Propulsion Laboratory, California Institute of Technology, 4800 Oak Grove Drive, Pasadena, California, USA.

Correspondence to: M. le Breton (Michael.le.breton@gu.se)

Abstract. Nitryl Chloride (ClNO₂) accumulation at night-time acts as a significant reservoir for active chlorine and impacts the following day's photochemistry when the chlorine atom is liberated at sunrise. Here, we report simultaneous measurements of N₂O₅ and a suite of inorganic halogens including ClNO₂ and Cl-VOCs in the gas and particle phase utilizing the FIGAERO-ToF-CIMS during an intensive measurement campaign 40 km Northwest of Beijing in May and June 2016. A maximum mixing ratio of 2900 pptVppt of ClNO₂ was observed with a mean campaign night-time mixing ratio of 487 ppt, appearing to have an anthropogenic source supported by correlation with SO₂, CO and benzene, which often persisted at high levels after sunrise until midday. This was attributed to such high mixing ratios persisting after numerous e-folding times of the photolytic lifetime enabling the chlorine atom production to reach 2.3 x 10⁵ molecules cm⁻³ from ClNO₂ alone, peaking at 9:30 am and up to 8.4 x 10⁵ molecules cm⁻³ when including the supporting inorganic halogen measurements.

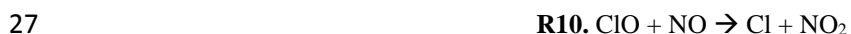
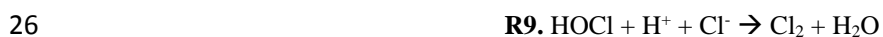
Cl-VOCs were ~~measured~~observed in the particle and gas phase for the first time at high time resolution and illustrate how the iodide ToF-CIMS can detect unique markers of chlorine atom chemistry in ambient air from both biogenic and anthropogenic sources. Their presence and abundance can be explained via time series of their measured and steady state calculated precursors, enabling the assessment of competing OH and chlorine atom oxidation via measurements of products from both of these mechanisms and their relative contribution to SOA formation.

1

2 1. Introduction

3 NO and NO₂ (NO_x) are important catalysts in the photochemical production of ozone (O₃) playing a significant
4 role in the oxidation of volatile organic compounds (VOCs) and subsequently have an adverse effect on air quality.
5 In the daytime NO_x is primarily removed by the hydroxyl radical (OH) to form nitric acid (HNO₃), which is
6 subsequently lost by wet deposition, becoming a major component of acid rain. At night-time, the OH radical is
7 not a significant oxidant as photolysis stops, enabling the reaction between NO₂ and O₃ to form significant levels
8 of the nitrate radical (NO₃) (Atkinson, 2000). NO₃ can accumulate at night or further react with NO₂ leading to the
9 formation of N₂O₅ (Brown *et al.*, 2003b, Brown and Stutz, 2012). This equilibrium can lead to the reaction of NO₃
10 with VOCs at night forming organic nitrates or act as an important intermediate for heterogeneous reaction on
11 aerosols as N₂O₅ produces NO₃⁻ and NO₂⁺ in the aqueous phase (Hallquist *et al* 1999, Hallquist *et al.*, 2000, Wagner
12 *et al.*, 2013). In the presence of chlorine, which is assumed in models to predominantly come from sea salt (Baker
13 *et al.*, 2016), nitryl chloride (ClNO₂) can be formed and released into the gas phase from the aerosol surface
14 (Osthoff *et al.*, 2008). ClNO₂ formation thereafter acts as a night-time radical reservoir due to its stability at night.

15 At sunrise ClNO₂ is rapidly photolysed, liberating the highly reactive chlorine atom subsequently converting it
16 into ~~Cl~~-ClO, HOCl and ClONO₂ depending on the available sunlight, O₃, HO_x and NO_x levels via the following
17 reaction pathways (R1-R11).

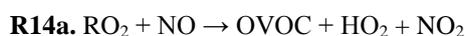
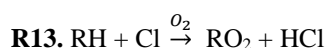
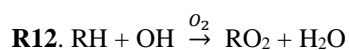


29

30 The liberated chlorine will predominantly react with VOCs, with the ~~above~~ pathways listed (R2-R11) representing
31 alternative routes to loss of the chloride ~~atom~~radical, and contribute to daytime photochemical oxidation,

1 competing with OH and perturbing standard organic peroxy radical abundance ($RO_x = OH + HO_2 + RO_2$), O_3
 2 production rate, NO_x lifetime and partitioning between reactive forms of nitrogen (Riedel et al., 2014). The
 3 ~~chlorine atom possesses~~ rate constants for the reaction of chlorine atoms with a number of VOCs is round 200
 4 times larger than the equivalent reaction with OH (Tanaka *et al.*, 2003); therefore, its abundance, fate and cycling
 5 can significantly alter standard daytime oxidation pathways. The oxidation of VOCs by chlorine atoms is thought
 6 to be significant in the early hours of the day while OH mixing ~~ratios~~ are low and chlorine atom production is
 7 high through the photolysis of $ClNO_2$, as well as feeding into the standard HO_x/NO_x cycles via production of
 8 peroxy radicals from reactions with alkanes. Additional Cl_2 photolysis and HCl reaction with OH can also produce
 9 chlorine atoms throughout the day but at lower rates.

10 ~~The oxidation mechanism of saturated hydrocarbon (R12-R13) is initiated~~ Saturated hydrocarbons are usually
 11 oxidised by reaction with OH or chlorine atom to form an organic peroxy radical (RO_2), and H_2O or HCl depending
 12 on the oxidant, (R12 and R13), which is the dominant pathway for chloride-VOC reactions. In a heavily polluted
 13 environment such as Beijing, the RO_2 favours further reactions with NO to form an oxygenated volatile organic
 14 compound, HO_2 and NO_2 or an alkyl nitrate $RONO_2$. Specifically, acyl peroxy radicals can also react with NO_2 to
 15 form acyl peroxy nitrates (APN) such as peroxy acetyl nitrate (PAN).



21 Addition of the chlorine atom to unsaturated VOC can also occur and then continue on the similar reaction pathway
 22 as denoted by R12 – R15. These pathways result in the production of unique chlorine atom chemistry markers
 23 which have been previously investigated to indicate the extent of chlorine atom oxidation reactions (Riemer *et al.*,
 24 2008, Keil and Shepson, 2006). The utilization of these compounds, such as 2-chloroperoxypropionyl nitrate (2-
 25 Cl PPN) and 1-chloro-3-methyl-3butene-2-one (CMBO) as chlorine atom chemistry markers relies on the
 26 abundance of the chlorine atom, the VOC precursor; HO_x , NO_x and O_3 and competing pathways for chlorine atom
 27 reactions. Riedel *et al.* (2014) calculated that up to ~~tens of ten parts per trillion~~ (ppt) Cl-VOCs are formed as a
 28 result of chlorine atom addition to alkenes and can therefore provide a number of potential periods of dominating
 29 active Cl chemistry (Wang *et al.*, 2001).

30 The production of chloroperoxy radicals via chlorine atom addition can lead to the formation of semi volatile
 31 oxidation products which have been observed for both biogenic (Cai and Griffin *et al.*, 2006) and anthropogenic
 32 emissions (Huang *et al.*, 2014, Riva *et al.*, 2015) in controlled laboratory studies. Chlorine initiated oxidation of
 33 isoprene could also represent a significant oxidation pathway due to its rapid reaction rate compared ~~to~~ with OH
 34 (Orlando *et al.*, 2003) resulting in gas phase products such as chloroacetaldehyde and CMBO, a unique tracer for
 35 atmospheric chlorine atom chemistry (Nordmeyer *et al.*, 1997). Furthermore, reactions of the chlorine atom with

1 isoprene or its SOA derived products could serve as an atmospheric chlorine sink (Ofner *et al.*, 2012). Wang *et al.*
2 (2017) revealed chlorine initiated oxidation of isoprene can produce SOA yields up to 36%, with products similar
3 to that of OH isoprene oxidation, compared ~~to~~with the 15% yield from standard oxidation calculated by Liu *et al.*
4 (2016), although this is known to be a factor of 2 higher than utilised in standard climate models. This SOA
5 formation from chlorine initiated oxidation presents a large knowledge gap in the literature, which to date is limited
6 by measurement capabilities.

7 This complex system results in a large uncertainty in the global budget of chlorine atoms $\sim 15\text{--}40\text{ Tg Cl yr}^{-1}$
8 calculated by indirect means (Allan *et al.*, 2007; Platt *et al.*, 2004), which is further limited by the ability of
9 measurement techniques to accurately quantify short lived species at low mixing ratios. Our knowledge of the Cl
10 budget therefore depends on the accurate measurement of its precursors, namely ClNO₂ and major reaction
11 pathways of the chlorine atom upon liberation in the daytime. Measurements to date show that the mixing ratio of
12 ClNO₂ vary geographically from below limits of detection to hundreds of ppt (Mielke *et al.*, 2015, Phillips *et al.*,
13 2012, Bannan *et al.*, 2015) and up to 3 parts per billion (ppb) (Tham *et al.*, 2014, Riedel *et al.* 2014, Liu *et al.*,
14 2017) in heavily polluted urban areas. To date, the majority of these measurements have been performed in the
15 United States, although with more recent research globally and in Europe, China have recently been published etc.
16 (Tham *et al.*, 2014, T Wang *et al.*, 2016, X. Wang *et al.*, 2017, Z. Wang, Liu *et al.* 2017). A major factor in the
17 variation of ClNO₂ mixing ratios is the availability and abundance of aerosol chloride which can vary significantly,
18 although is predominantly present as sodium chloride from sea salt.

19 Iodide adduct ionization has previously been applied to measure inorganic halogens in ambient air (Osthoff *et al.*,
20 2008, Riedel *et al.*, 2012, Thornton *et al.*, 2010, Le Breton *et al.*, 2017a) using mass spectrometers with quadrupole
21 mass analysers. This technique involves periodically changing the tuning of the spectrometer to allow transmission
22 of a particular mass ion to the detector. Several species are therefore often “chosen” for detection in order to
23 achieve high enough time resolution. Recent developments and availabilities of a Time of Flight Chemical
24 Ionisation Mass Spectrometer (ToF-CIMS) have enabled the simultaneous measurement of all detectable ions by
25 an ionization technique via high frequency full mass spectral collection. The high resolving power (3500) of this
26 technique also enables much lower limits of detection for species which may have the similar mass to a compound
27 that is much more abundant via multi peak fitting. This technique has previously been applied for the measurement
28 of ClNO₂ and Cl₂ (Faxon *et al.* 2015) and recently for Cl-VOCs (Wang *et al.*, 2017) in the gas phase. In this study,
29 a ToF-CIMS utilizing the FIGAERO (Filter Inlet for Gas and AEROsols) is deployed at a site in semi-rural Beijing,
30 China to measure the gas and particle phase precursor (ClNO₂, N₂O₅) and selective halogen containing species at
31 high time frequency and resolving power to further our understanding of the chlorine atom budget in this region
32 and its potential fate.

33

34 2. Experimental

35 2.1 Site description

36 The data presented here ~~was~~were collected during the inter-collaborative field campaign, within the framework of
37 a Sino-Sweden research project “Photochemical Smog in China” aimed to further our understanding of the episodic

1 pollution events in China through gas and particle phase measurements with numerous analytical instruments. The
2 laboratory setup in the Changping University Campus of PKU was situated at a semi-rural site 40 km North West
3 of Beijing close to Changping town (40.2207° N, 116.2312° E). The general setup has previously been described
4 by Le Breton *et al.*, 2017b.

5
6 All instruments sampled from inlets setup in a laboratory 12 metres high from the 13th May 2016 to 23rd June 2016.
7 The site has a small town within its vicinity and some small factories within 5 kilometers. A High Resolution Time
8 of Flight Aerosol Mass Spectrometer (HR-ToF-AMS) was utilized to measure the mass mixing ratios and size
9 distributions of non-refractory species in submicron aerosols, including organics, sulfate, ammonium and chloride
10 (DeCarlo *et al.*, 2006, Hu *et al.*, 2013). The setup of this instrument has been previously described by Hu *et al.*,
11 (2016). Photolysis rates were measured by a commercial spectradiator for O₃, NO₂, HCHO, HONO and H₂O₂-
12 (Metcon UF CCD), the instrument was calibrated by high power halogen lamp after the field campaign. The
13 photolysis rate of any given other related species was calculated by normalizing to the cross section and quantum
14 yields taken from the recommendations were scaled by the recommendation of the Jet Propulsion Laboratory (JPL)
15 kinetic evaluation report (Burkholder *et al.*, 2015). Before the campaign the was instrument calibrated through
16 comparison with a chemical actinometer in 2014 (Zou *et al.*, 2016).

17 An Ionicon Analytik high sensitivity PTR-MS (Proton TRansfer Mass Spectrometer) as described by de Gouw
18 and Warneke *et al.*, (2007) provided supporting precursor VOC measurements. Detailed information about the PTR
19 MS measurements can be found in Yuan *et al.* 2012 and 2013. In brief, 28 masses are measured for throughout the
20 campaign at 1 Hz. Zero air, which was produced by ambient air passing through a platinum catalytic converter at
21 350 °C (Shimadzu Inc., Japan), was measured for 15 min every 2.5 hours to determine the background. used to
22 measure background Aromatics Aromatic masses (m/z 79 for benzene, m/z 93 for toluene, m/z 105 for styrene,
23 m/z 107 for C₈ aromatics and m/z 121 for C₉ aromatics), oxygenated masses (m/z 33 for methanol, m/z 45 for
24 acetaldehyde, m/z 59 for acetone, m/z 71 for MVK+MACR and m/z 73 for MEK), isoprene (m/z 69) and
25 acetonitrile (m/z 42) were calibrated by using EPA TO15 standard from Apel-Riemer Environmental Inc., USA.
26 Formic acid (m/z 47), acetic acid (m/z 61), formaldehyde (m/z 31), and monoterpenes (m/z 81 and m/z 137) were
27 calibrated by permeation tubes (VICI, USA). The uncertainties of most species are below 10%, which is detailed
28 in the previous work (Liu, Y. 2015, ACP).

29 30 **2.2 ToF-CIMS setup**

31 Gas and particle phase ambient species were measured using an iodide ToF-CIMS (resolving power of 3500)
32 coupled to the FIGAERO inlet (Lopez-Hilfiker *et al.*, 2014). The setup for this campaign has previously been
33 described by leLe Breton *et al.* (2017b). Briefly, the iodide ionization scheme was utilised to acquire non-
34 fragmented ions of interest by passing UHP N₂ over a permeation tube containing liquid CH₃I (Alfa Aesar, 99%),
35 and through a Tofwerk X-Ray Ion Source type P (operated at 9.5 kV and 150 μA) to produce the iodide reagent
36 ions. The ionized gas was then carried out of the ion source and into the Ion-Molecule Reaction (IMR) chamber,
37 which was heated to 40 degrees Celsius to reduce wall loss, through an orifice (Ø = 1 μm). The inlet lines were 2
38 metres long and composed of copper tubing (12 mm) for the aerosol inlet and Teflon tubing (12 mm) for the gas
39 sample line. Particles were collected onto a Zefluor® PTFE membrane filter at the same rate as the gas inlet line

1 sampling, 2 SLM. The FIGAERO was operated in a cyclic pattern; 25 minutes of gas phase measurement and
2 simultaneous particle collection, followed by a 20 minute period during which the filter was shifted into position
3 over the IMR inlet and the collected particle mass was desorbed.

5 2.3 Calibration

6 In the field formic acid calibrations were performed daily utilising a permeation source maintained at 40 °C. A dry
7 N₂ flow (200 sccm) was passed over the permeation source and joined a 2 SLM N₂ flow line directed towards the
8 inlet. The mixing ratio of the flow was determined by mass loss in the laboratory after the campaign. The sensitivity
9 of the ToF-CIMS to formic acid was found to be 3.4 ion counts per ppt Hz⁻¹ for 1x10⁵ iodide ion counts.

10 N₂O₅ was synthesized by mixing 20 ppm O₃ with pure NO₂ (98%, AGA Gas) in a glass vessel and then passing
11 the mixture through a cold trap held at -78.5 °C by dry ice. The N₂O₅ was transferred to a diffusion vial fitted with
12 a capillary tube (i.d. 2 mm). The N₂O₅ diffusion source was held at a constant temperature (-23 °C), and the mass
13 loss rate was characterized gravimetrically for a flow rate of 100 sccm. The same flow was added to a dry nitrogen
14 inlet dilution flow of 2 SLM to calibrate the CIMS. ClNO₂ measurements were quantified by passing the N₂O₅
15 over a wetted NaCl bed to produce ClNO₂. The decrease in N₂O₅ from the reaction with NaCl was assumed to be
16 equal to the mixing ratio of ClNO₂ produced (i.e., a 100% yield). Conversion of N₂O₅ to ClNO₂ can be as efficient
17 as 100% on sea salt, but it can also be lower, for example if ClNO₂ were to convert to Cl₂ (Roberts et al., 2008).
18 For NaCl the conversion efficiency has however been as low as 60% (Hoffman et al., 2003). In this calibration we
19 have followed the accepted methods of Osthoff et al., (2008) and Kercher et al., (2009) that show a conversion
20 yield of 100% and have assumed this yield in the calibrations of this study. The lower detection limit of the CIMS
21 to N₂O₅ and ClNO₂ was found to be 9.5 and 1.2 ppt respectively for 1 minute averaged data. ~~Using the~~The error in
22 the individual slope of the calibrations results ~~in yields~~ a total uncertainty of 30% for both N₂O₅ and ClNO₂. These
23 sensitivities for N₂O₅ and ClNO₂ (9.8 and 1.6 ion counts per ppt Hz⁻¹ for ~~1x10⁵~~ 1 x 10⁵ iodide ion counts) were
24 applied relatively to that of formic acid. The other inorganic halogens reported in this work are ~~assumed to have~~
25 ~~the same sensitivity as ClNO₂. This is in line with that Le Breton et al. (2017) reported many inorganic halogens~~
26 ~~possess a similar, if not the same, sensitivity, which is also supported by our chloroacetic acid calibration reported~~
27 ~~in ion counts.~~ Other acids identified by CIMS which are reported in the literature are given the sensitivity of N₂O₅
28 to provide a minimum concentration so no concentrations are over estimated.

29 A post campaign calibration of chloroacetic acid (99%, Sigma Aldrich) was utilised to ~~apply~~characterise a
30 sensitivity factor for ~~all~~ Cl-VOCs measured during the campaign VOC. The calibration was performed using the
31 same method as for formic acid and gave a sensitivity of 1.02 ion counts ppt⁻¹ Hz when normalized to ~~1x10⁵~~ 1 x
32 10⁵ I⁻ ion counts. ~~Using This similar sensitivity to that of the Cl VOC to that of ClNO₂ could imply a relative~~
33 ~~sensitivities will increase the uncertainties, but is a commonly applied method with~~sensitivity may be appropriate
34 ~~to constrain the CIMS community mixing ratios of all Cl VOCs, although in further work is required to confirm~~
35 ~~this specific case it is very likely that and therefore the sensitivity is similar for all inorganic/organic halogens, as~~
36 ~~demonstrated by Le Breton et al. (2017a)-manuscript reports all Cl VOC measurements in units of ion counts.~~

1 2.4 Model setup

2 The EMEP MSC-W chemical transport model (Simpson et al., 2012, Simpson et al., 2017) driven by meteorology
3 from the WRF-ARW model (Skamarock et al., 2008) was utilised to support source analysis of the particulate
4 chloride. The model was run on two nested domains (0.5° and 0.1667° resolution respectively) with biomass
5 burning emissions from the two databases FINN and GFAS, and anthropogenic emissions from the MEIC
6 inventory (<http://meicmodel.org/>). Two versions of the model, one getting emissions from open biomass burning
7 from the Fire Inventory from NCAR (FINN) (Wiedinmyer et al., 2011) and one getting them from the Global Fire
8 Assimilation System (GFAS) (Kaiser et al., 2012), were run for the entire period of the Changping measurement
9 campaign.

10 Results and Discussion

11 3.1 Peak identification and quantification

12 Peak fitting was performed utilizing the Tofware peak fitting software for molecular weights up to 620 AMU. The
13 standard peak shape was fitted a peak on the spectra until the residual was less than 5%. Each unknown peak was
14 assigned a chemical formula using the peaks exact mass maxima to 5 decimal places and also isotopic ratios of
15 subsequent minor peaks. An accurate fitting was characterized by a ppm error of less than 5 and subsequent
16 accurate fitting of isotopic peaks. The analysis here focuses on species identified in the mass spectra considered to
17 possibly play important roles with respect to the night-time chlorine reservoir and several other key night-time
18 oxidants; ClNO₂, HCl, Cl₂, ClO, HOCl, OClO, ClONO₂, N₂O₅ and Cl-VOCs. Figure 1 displays the average mass
19 spectra for the measurement campaign and the peak fitting applied for ClO and ClNO₂. All species were
20 [represented by](#) a dominant peak with a multi peak fit, although a number of co-existing peaks were present for
21 much of the campaign. This signifies the importance of high resolution fit data and the need for high resolution
22 measurements. A quadrupole CIMS may not be able to resolve the peak adjacent to ClO at m/z 178 (dominant
23 peak is IC₆F₃HO₃⁻) and the second dominant peak for the ClNO₂ fit (cluster of HNO₃ with water) would result in
24 a 10% over estimation.

25

26 3.2 N₂O₅ measurements

27 The CIMS and a Cavity Enhanced Absorption Spectrometer (CEAS) measured N₂O₅ (Wang *et al.*, 2017)
28 simultaneously from the 13th May 2016 to the 6th June 2016. However, given the use of the FIGAERO, the CIMS
29 alternated measurements between gas and particle phases so did not generate a completely continuous gas phase
30 time series. Here, the CEAS is utilised to validate the CIMS N₂O₅ (at m/z 235) measurements and also instrument
31 stability. The CEAS utilised a dynamic source by mixing NO₂ and O₃ to generate stable N₂O₅ for calibration (Wang
32 *et al.*, 2017). The source was used to calibrate the ambient sampling loss of N₂O₅ in the sampling line, filter, the
33 preheater cavity and optical cavity. This was performed pre and post campaign. During the campaign the
34 reflectivity of the high reflectivity mirror was calibrated daily and filter changed hourly. The simultaneous
35 measurements of N₂O₅ can be shown in Figure 2 for one minute averaged data. The time series [show-ashows](#) good
36 agreement for both background mixing ratios during the day (sub 10 ppt) and high night-time mixing ratios (up to

1 800 ppt), excluding one night. The highest N₂O₅ levels observed by both the CEAS and CIMS were observed on
2 the 3rd June although the CEAS reports 880 ppt whereas the CIMS reports 580 ppt. If included in the analysis the
3 R² is 0.71 and when excluded it is 0.76. To date the reason for this deviation during that night is not known but it
4 should be stressed that N₂O₅ measurements are delicate and highly ~~depending~~dependent on sampling condition,
5 e.g. the RH. Nevertheless, excluding this night from the comparison, a slope of 0.85 is observed and a ~~yan~~ offset
6 of 0.9 ppt. The diurnal profile in Figure 2 represented the difference between the two measurements throughout
7 the campaign. The largest error between the two measurements occurs at night during the higher levels of N₂O₅,
8 although averaging at 4 ppt (representing 11% error on the average campaign concentration). Differences could
9 arise from a number of various factors. Inlet differences such as the CIMS heated IMR (to 40 °C to reduce wall
10 loss), residence time and ambient NO₂ can all change thermal decomposition and wall loss rates between the
11 instruments, which is determined for the CEAS in Wang *et al.* (2017) but not for the CIMS in this work. Also, the
12 separate inlets were facing in different directions within the same laboratory, possibly enabling local wind patterns
13 to affect the mixing ratios reaching each instrument.

14 The CEAS data was further utilised to assess any sensitivity changes for the CIMS that daily carboxylic acid
15 calibrations did not account for. A time series of hourly factor differences between the CIMS and CEAS was
16 implemented into ~~these~~ data to weight the measurements to a normalised sensitivity. The high level of
17 agreement (R² of 0.76) from low mixing ratio measurements and a species with a short lifetime from different
18 inlets confirms the accuracy and reliability of the CIMS measurements for this campaign.

19 Generally, N₂O₅ was detected throughout the campaign with a clear diurnal variation peaking at night-time and
20 rapidly falling to below limits of detection in the daytime as a result of photolysis of N₂O₅ and NO₃. The campaign
21 mean night-time mixing ratio was 121 ppt with a standard deviation of 76 ppt. The maximum mixing ratio of N₂O₅
22 observed was 880 ppt on the 3rd June. This range of mixing ratios lie within the recently reported values in the
23 literature, but not at the extreme mixing ratios as observed in Germany (2.5 ppb) (Phillips *et al.*, 2016) or Hong
24 Kong (7.7 ppb) by Wang *et al.* (2016) and Brown *et al.* (2017). Although the mean mixing ratios do not increase
25 significantly during the pollution episodes, the maximum mixing ratios detected overnight increase by up to a
26 factor of 4. Further analysis of N₂O₅ nighttime chemistry was performed by Wang et al (2018) who calculated an
27 average steady state lifetime of 310 + 240 s and mean uptake coefficient of 0.034 ± 0.018.

28

29 **3.3 Inorganic chlorine: Abundance, profiles and source**

30 **3.3.1 Abundance and profiles**

31 Mean diurnal profiles of HCl, Cl₂, ClONO₂, HOCl, ClO and ClNO₂ are displayed in Figure 3 from data between
32 the 23rd May and the 6th June. HCl exhibited a standard diurnal profile increasing in mixing ratio throughout the
33 day and peaking at 4 pm which then fell off slowly at night. The mean HCl campaign mixing ratio was 510 ppt
34 (standard deviation (σ) 270 ppt) and the maximum HCl mixing ratio was 1360 ppt on the 30th June. Cl₂ exhibited
35 a diurnal profile peaking at both ~~the~~ night-time and daytime. High mixing ratios were observed at night followed
36 by a sharp loss at sunrise and a general build-up throughout the day. The campaign mean mixing ratio was 0.65
37 ppt (σ 0.5 ppt) and the maximum mixing ratio was 4.2 ppt on the 4th June just before midnight. This agrees well

1 with recent urban measurements of Cl₂ in the USA where Faxon et al. (2015) observed a maximum of 3.5 ppt and
2 Finley et al. (2006) observed up to 20 ppt in California. Up to 500 ppt Cl₂ has recently been reported in the Wangdu
3 County, South West of Beijing (Liu et al., 2017). Although the mixing ratios we report here are significantly lower,
4 as detailed later, their source ~~maybe~~ may be of similar origin, which is indicated to be from power plant emissions.

5 The diurnal profile of HOCl peaked during the daytime via its main formation pathways are via reaction of ClO
6 and HO₂ and Cl with OH. Interestingly, the ClO in this work exhibits a night-time diurnal peak, contradicting
7 known formation pathways via Cl reaction with O₃ and the photolysis of ClONO₂. The complexity continues as
8 ClONO₂ also peaks during the night, given that its main known formation pathway is via reaction of ClO (produced
9 at sunrise via ClNO₂ photolysis) with NO₂. The misidentification of ClONO₂ and ClO is not thought to be a
10 possible reason for these discrepancies due to the low number of mass spectral peaks that have maxima at night
11 and the mass defect of chlorine making the peak position unique to chlorine containing molecules. IMR chemistry
12 is also not a possible source as these reactions would occur throughout the day, therefore skewing all of the data
13 and not just the night-time levels, although there is a possibility that ClONO₂ can be formed in the IMR by reactions
14 between ClO and NO₂. It is hypothesized that in extremely high OH and HO₂ mixing ratios, all ClO is rapidly
15 converted to HOCl, limiting the formation on significant levels of ClO and subsequently ClONO₂. Khan et al
16 (2008) suggest that Cl atoms of around ~~2x1042~~ 2×10^4 molecules cm⁻³ could be present at night via analysis of
17 alkane relative abundance. Although a formation mechanism is not proposed, it provides further evidence that ClO
18 formation at night-time is possible and may represent an unknown reaction pathway, which would agree with the
19 measurements presented in this work.

20 ClNO₂ exhibited a similar diurnal profile as N₂O₅, peaking at night-time and lost during daylight due to photolysis.
21 The campaign mean night-time mixing ratio was 487 ppt. The maximum mixing ratio observed was 2900 ppt on
22 the 31st May, similar to that previously measured at semi-rural site in Wangdu (up to 1500 ppt) (Liu et al., 2017),
23 Mount Tai (2000 ppt) (Wang et al., 2017), but lower than that in Hong Kong (4 ppb) (Wang et al 2016).

25 3.3.2 Source of chloride

26 The high levels of ClNO₂ indicate a local significant source of chlorine to support these observations. The
27 dominant source of chlorine atoms for ClNO₂ production within models, such as the Master Chemical Mechanism
28 (MCM), is from sea salt. However, the site is situated 200 km from the Yellow Sea and therefore this origin would
29 have a low probability. The mean AMS chloride mass loading was 0.05 µg m⁻³ for the campaign with a maximum
30 of 1.7 µg m⁻³. The Cl⁻ from the AMS appears to be correlated strongly with CO and SO₂, possibly originating from
31 power plants or combustion sources. It should be noted that the AMS data does not include refractory aerosol and
32 also has a cut off size larger than ~~anticipate~~ the anticipated size of sea salt particles. Instead, the high Cl⁻ observed
33 appears to originate from mainland areas to the site (Figure 4) rather from the nearest coast, further supporting a
34 ~~strong~~ anthropogenic source. Tham et al., (2016) observed a strong correlation of aerosol chloride with SO₂ and
35 potassium from measurements done during the same season in 2014 at Wangdu (semi-rural site 160 km south
36 West of Beijing) and suggested ~~contribution~~ contributions to fine chloride from burning of coal and crop residues.
37 The latter was also supported by satellite fire spot count data (Tham et al., 2016). Riedel et al. (2013) have
38 previously reported high ClNO₂ mixing ratios observed from urban and power plant plumes measuring high mixing

1 ratios of gas phase Cl_2 . The correlation with SO_2 indicates coal burning as a potential source of particulate chlorine
2 which is known to be a significant source of PM in the Beijing region (Ma et al., 2017), and the correlation with
3 CO and benzene could be an indicator of biomass burning (Wang et al., 2002). To support this analysis, figure S1
4 displays a wind rose plot in which radial and tangential axes represent the wind direction and speed (km h^{-1}). The
5 colour bar represents the $\text{PM}_{2.5}$ concentration. We could see that during the campaign, the severe pollution was
6 from the south and southwest, with little contribution from the east part. Therefore, ~~we could deduce~~ it is likely that
7 little contribution of the chloride was from the ocean.

8 In order to test the hypothesis of biomass burning as a source of particulate chlorine, biomass burning emissions
9 and transport utilising the EMEP MSC-W chemical transport model driven by meteorology from the WRF-ARW
10 model (Skamarock et al., 2008) were used. Neither of the two biomass burning databases used (FINN and GFAS)
11 contained data on chlorine emissions, so instead the biomass burning emissions of CO (CO_{bb}) were tracked and
12 compared ~~to~~ with the total mixing ratio of CO (CO_t) at the Changping site. CO was chosen since the measurements
13 at Changping had shown a strong correlation between CO and ClNO_2 and because CO could be expected to be co-
14 emitted with chlorine for both biomass burning and industrial combustion.

15 Figure S2 (supplementary) shows the time series of the measured ClNO_2 mixing ratios at the Changping site, as
16 well as the modelled mixing ratios of CO_t and CO_{bb}. CO_{bb} is shown for calculations using either the FINN or the
17 GFAS data base, while for clarity the CO_t is only shown using the FINN data base. ~~From this figure it~~ It is clear
18 that mixing ratios of CO_{bb} are very low compared ~~to~~ with CO_t. ~~(figure S2)~~. The two pollution episodes on May
19 18-May 23 and May 28-June 5, are to some extent visible in all time series, but for the biomass burning CO series,
20 the second episode is much less pronounced. Night-time averages of the mixing ratios shown in figure S2 were
21 calculated for each night for the time period 18:00 to 08:00 local time (UTC+8), roughly corresponding to the
22 period when ClNO_2 is not destroyed by photolysis. Nights with significant amount of missing data for the
23 measurements were excluded. Figure S2 shows scatter plots of these averages of ClNO_2 against the averages of
24 the other species including their linear fits. The R^2 value for these fits were 0.48, 0.04, and 0.21 for CO_t, CO_{bb}
25 FINN, and CO_{bb} GFAS respectively. The fact that mixing ratios of CO_{bb} is ~~are~~ so much smaller than CO_t
26 according to the model, combined with the much better correlation for CO_t than for CO_{bb} strongly suggests that
27 industrial emissions are the dominant source of chlorine, rather than biomass burning. To further investigate the
28 source of chloride, the model was also run to calculate sea salt levels instead of CO. This resulted in a poor
29 correlation between sea salt and the ClNO_2 (figure S4). The absolute levels of sea salt calculated by the model
30 were also very low, unlikely to be able to produce the observed mixing ratios of ClNO_2 as observed by CIMS.

32 3.4 Particle phase ClNO_2

33 A particle desorption profile was observed in the high resolution data for ClNO_2 . The count increase at this 1 AMU
34 mass can be attributed to two sources; SO_3 and ClNO_2 as shown in Figure 5. The SO_3 peak is predominantly found
35 in the particle phase and is below the limit of detection (LOD) in the gas phase. During initial analysis of ~~the~~ these
36 data, SO_3 interfered with the ClNO_2 peak fitting and attributed its counts to ClNO_2 in the particle phase as its ^{33}S
37 ion is only 0.005 AMU away from the ClNO_2 peak. Upon its inclusion into the peak list and utilisation of the
38 Tofware feature which constrains isotopes and reallocates the signal appropriately, ClNO_2 remains to indicate a

1 strong desorption profile. The diurnal cycle of these desorptions correlate well with the ClNO₂ gas phase profile,
2 indicating a correct assignment of the counts to particle phase ClNO₂. The desorption profiles with respect to
3 temperature also exhibit a thermogram structure and not e.g. for example a gas phase leak into the system which
4 could have accounted for the correlation with the gas phase time series. This suggests the possible presence of
5 ClNO₂ in the particle phase. Another possible explanation could be the deposition of ClNO₂ from the gas phase
6 onto the filter as the ambient air flows through the FIGAERO.

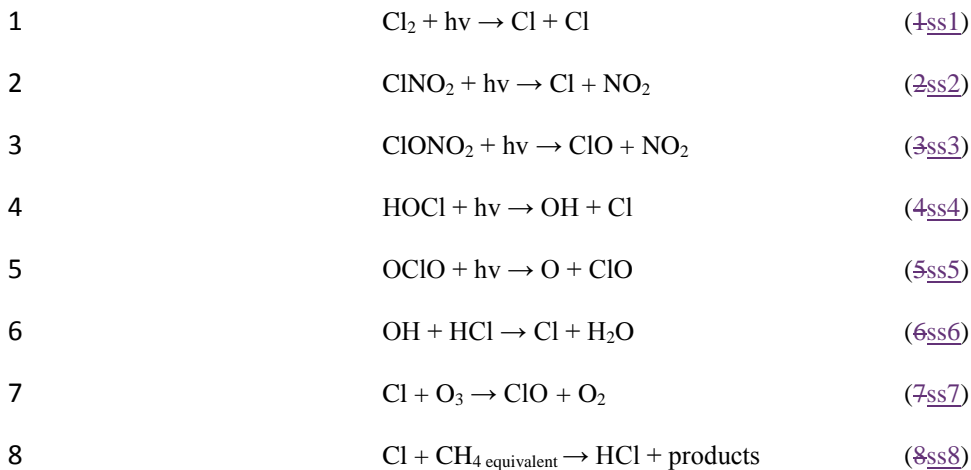
7 If we assume the analysis and collection technique is correct, we see an average particle to gas phase partitioning
8 of 0.07, with a maximum of 0.33 and a minimum of 0.009. The average mixing ratio of ClNO₂ collected onto the
9 filter during desorption is 13 ppt with a maximum of 120 ppt. Previous modelling studies assume all ClNO₂ is in
10 the gas phase due to the low Henry's law constant e.g. for the TexAQS II campaign they calculated that 0.1 ppb
11 in the gas phase would yield 0.54 ppt in the particle phase (Simon *et al.*, 2008). However, thisthese data
12 indicatessuggests that a non-negligible amount of the chlorine associated with ClNO₂ is not liberated from the
13 particle phase, assuming that no additional ClNO₂ is formed by thermally driven reactions. The slope of the particle
14 to gas phase CIMS data is calculated to be 0.048, a factor of 96 higher than using the Henry's law coefficient to
15 estimate the particle mixing ratio.

17 3.5 ClNO₂ daytime persistence and Cl liberation

18 Both ClNO₂ and N₂O₅ are photolytically unstable, with studies reporting lifetimes on the order of hours for ClNO₂
19 depending on the solar strength (e.g. Ganske *et al.*, 1992, Ghosh *et al.*, 2011). Nocturnal ClNO₂ removal pathways
20 have generally been reported to be negligible, with ClNO₂ being assumed to be relatively inert (Wilkins *et al.*,
21 1974; Frenzel *et al.*, 1998; Rossi, 2003; Osthoff *et al.*, 2008), but the work of Roberts *et al.*, (2008) and Kim *et al.*,
22 (2014) would suggest that this may not be strictly true. However, given that the average diurnal profile does not
23 show the importance of nocturnal removal pathways in this study, observed losses are attributed solely to
24 photolysis, with J(ClNO₂) controlling the lifetime.

25 Rapid photolysis can be observed for N₂O₅ in Figure 6 showing a near instant drop below LOD, whereas the ClNO₂
26 mixing ratio not only persists for up to 7 hours, but also shows evidence of an increase in mixing ratio at 7 am
27 (Figure 6). This is observed throughout the campaign and has been frequently observed in the previous study at
28 Wangdu (Tham *et al.*, 2016). The breakdown of the nocturnal boundary layer and inflow of air masses from above,
29 carrying pollution from nearby industry/ies is a likely cause of this persistence of possible increase of ClNO₂. Liu
30 *et al.* (2017) also observed high daytime mixing ratios of ClNO₂ (60 ppt) at the Wangdu site which they attribute
31 to a possible oxidation mechanism due its correlation with O₃ and Cl₂ providing a daytime formation pathway to
32 maintain mixing ratios against its rapid photolysis.

33 Consistent with past measurements and the measurements of this study, ClNO₂ is expected to provide a significant
34 source of Cl during day time hours, presenting a potentially significant source of the reactive Cl atom during the
35 day. Its rapid photolysis rate and elevated mixing ratios enables Cl to compete with OH oxidation chemistry, the
36 known dominant daytime radical source. Here, a simple steady state calculation will be used to determine the Cl
37 atom mixing ratio summarised belowas follows, but detailed within the supplementary:



9

10 $[\text{Cl}]_{\text{SS}} = \{2J_1[\text{Cl}_2] + J_2[\text{ClONO}_2] + J_3[\text{ClONO}_2] + J_4[\text{HOCl}] + J_5[\text{OCIO}] + k_7 [\text{OH}][\text{HCl}]\} / \{k_7[\text{O}_3] + k_8[\text{CH}_4_{\text{equivalent}}]\}$
 11 (9)

12 Where $[\text{CH}_4]_{\text{equivalent}}$ represents the reactive VOC present as if it were reacting as CH_4

13 Bannan et al., (2105), were able to use this steady state approach to compare the relative loss via reaction with OH
 14 compared with Cl atoms. Although this approach is an estimation, it was shown to produce results comparable to
 15 results with that of the more rigorous MCM approach, although we do acknowledge large errors will be present in
 16 the radical species calculations, which is detailed in the supporting information. Steady state calculations reveal a
 17 sharp rise of chlorine atoms produced at sunrise peaking at $1.6 \times 10^5 \times 10^5$ molecules cm^{-3} around 7 am which
 18 then gradually decreases, contributing to Cl atom production until 2 pm (Figure 7a). Supporting Cl_2 , ClONO_2 ,
 19 OCIO , HOCl and HCl measurements by CIMS report that chlorine atoms can sustain a relatively high production
 20 rate until 3 pm as evidenced by the daytime build-up of HCl and Cl_2 . ClONO_2 on average contributes ~~to~~ 78% of the
 21 chlorine atoms produced from inorganic halogens with 13% from Cl_2 . ClONO_2 also represents over 50% of the
 22 chlorine atoms until midday. After ca. 3 pm Cl_2 and HCl becomes the more dominant Cl atom ~~sources~~
 23 the night where the highest ClONO_2 mixing ratios were measured, 90% of the chlorine atoms originated from ClONO_2
 24 photolysis until 2 pm and HCl and Cl_2 then become main contributors ~~sustaining~~ until 4 pm (up to 80%). ClONO_2 ,
 25 HOCl and OCIO appear to be insignificant contributors to chlorine atom production throughout the campaign
 26 compared with ClONO_2 , HCl and Cl_2 .

27 To put these chlorine atom mixing ratios into a more global perspective, data collected by the University of
 28 Manchester from a marine site and an urban European site have been compared in Figure 7b. Bannan et al., (2015)
 29 and (2017) previously utilised a box model to calculate Cl atom mixing ratios during the campaign so that the rate
 30 of oxidation of VOCs by Cl atoms could be compared with oxidation by measured OH and measured ozone. The
 31 simple steady state calculation described previously will be used to determine the Cl atom mixing ratio for ~~both~~
 32 this measurement study. The results show that both at the UK marine and urban site ~~max~~ maximum chlorine atom
 33 mixing ratios are more than an order of magnitude lower than the mean of Beijing. It should ~~however~~ be noted that
 34 the only source of Cl in the UK studies was ClONO_2 , but given the dominance of ClONO_2 in this study the
 35 measurements presented here suggest a high importance of the chlorine chemistry for the Asian air chemistry.
 36 Studies of chloride chlorine radical production in Los Angeles by Riedel *et al.* (2012) and Young *et al.* (2014)

1 indicate that the high production rate in Beijing is somewhat typical of urban sites, although HCl and ClNO₂
2 contribution to radical production is the same, whereas here we see very little chloride radical production from
3 HCl in comparison ~~to~~with ClNO₂.

4 Although this study does not reach the scope of characterising O₃ and RO_x production from chlorine atom
5 chemistry, statistics are often reported with ClNO₂ morning chemistry via modelling simulations, we can put into
6 perspective the mean and maximum mixing ratios relative to other studies. Tham *et al.* (2016) recorded a maximum
7 ClNO₂ mixing ratio of 2070 ppt from a plume originating from Tianjin, the closest megacity to Beijing, and report
8 a 30% increase in RO_x production and up to 13% of O₃ production. Liu *et al.* (2017) observed peak mixing ratios
9 up to 3 ppb and similar diurnal mixing ratios which they calculated contributes to a 15% enhancement of peroxy
10 radicals and 19% O₃ production. Wang *et al.* (2016) report up to 4.7 ppb of ClNO₂ in Hong Kong and calculated
11 a maximum increase of 106% of HO_x in the morning and an enhancement of ~~following daytime~~O₃ production the
12 next day by up to 41%. ~~Therefore, it is therefore~~ evident that this work supports similar studies in Asia that
13 conclude that chlorine atom oxidation significantly contributes to atmospheric oxidation via RO_x and O₃
14 production. Although several studies have demonstrated a non-negligible impact of chlorine oxidation chemistry
15 (e.g. Oshoff *et al.*, 2008, Riedel *et al.*, 2014 and Sarwar *et al.*, 2014), the impact of Cl chemistry varies significantly
16 between various areas and atmospheric conditions, e.g. Bannan *et al.*, (2015, 2017) deemed the impact from
17 chlorine atom chemistry to be relatively low with respect to O₃ production and competing with OH radicals for
18 VOC oxidation²².

20 3.6 VOC oxidation by chlorine atoms

21 Steady state calculations of OH (as described by Whalley *et al.*, 2010) estimate that campaign average maximum
22 mixing ratio was 7 x 10⁶ molecules cm³ (Figure 7b), 6 times greater than the maximum chlorine atom mixing ratio
23 and 14 times higher than the average chlorine atom mixing ratio. Pszenny *et al.* (2007) report estimated OH to
24 chlorine atom ratios, from VOC lifetime variability relationships, of 45 to 199 along the East Coast of the United
25 States. Although the ratio appears much larger than calculated in this work, here we present not only significantly
26 highhigher mixing ratios of ClNO₂ which are appearing to be a consistent conclusion from measurements in Asia,
27 but also the chlorine within this study appears to originate from an anthropogenic origin rather than marine,
28 possessing the ability to supply a much larger reservoir of halogens to be liberated through photolysis.

29 The relative oxidation rate of the chlorine atom and OH to VOCs can vary greatly. Rate coefficients for reaction
30 of Cl atoms with some volatile organic compounds have been shown to be up to 200 times faster than the
31 comparable reaction with OH. The ratio reported here is significantly less than this each day, Cl can subsequently
32 dominate VOC oxidation for some fraction of the day. Here, the diurnal maxima of the chlorine atom and OH
33 differs by 5 hours, enabling chlorine atoms to clearlydominate VOC oxidation earlier in the day before OH mixing
34 ratios have built up. The relative oxidation rate of VOCs to OH and the chlorine atom also varies greatly, creating
35 a difference for various VOCs. If an average reaction rate for alkenes and alkanes to Cl and OH is calculated, it is
36 possible to generalise the significance of each oxidation pathway to qualitatively assess the contribution chlorine
37 atoms have on oxidation chemistry. It can be seen in Figure 8 that alkenes are much more likely to be oxidised by
38 OH than Cl, although a significant contribution (15%) is attributed to chlorine chemistry. Although significant if

1 evaluated on a global level, Liu *et al.*, (2017) estimated that Cl atoms oxidize slightly more alkanes than OH
2 radicals in a similar region of China, implying the increased scale of chlorine oxidation in China. Alkanes are
3 known to have a much higher Cl to OH relative reaction rate than alkenes and Cl contribution to oxidation is higher
4 than OH until midday. The contribution to oxidation remains almost equal for the remainder of the day due to the
5 persistence of ClNO₂ and also relatively high levels of Cl₂ and HCl. This analysis is representative of that by
6 Bannan *et al.* (2015) who report contributions of alkene and alkane oxidation by Cl up to 3 and 15% respectively
7 from ClNO₂ mixing ratios peaking at 724 ppt.

8 This significant oxidation of VOCs by chlorine atoms will result in different products to that of OH oxidation as
9 illustrated and that neglecting the contributions made by Cl atoms will significantly underestimate the degree of
10 chemical processing of VOCs in this study, and other environments where there is a source of Cl atoms. Evidence
11 of the proposed Cl oxidation of VOCs is validated through detection of selected Cl induced oxidation products by
12 the ToF-CIMS, all of which are displayed in Table 1.

14 3.6.1 Isoprene oxidation by the chlorine atom

15 1-Chloro-3-methyl-3-butene-2-one (CMBO, C₅H₆ClO), a unique marker of chlorine chemistry, has previously
16 been measured at mixing ratios up to 9 ppt by offline gas chromatography in Houston Texas (Tanaka *et al.*, 2003)
17 and in laboratory studies of chlorine-isoprene oxidation (Wang *et al.* (2017)). CMBO exhibited a campaign
18 maximum of ~~13.2 ppt~~21 and mean of ~~5.16 ppt~~34 ion counts (near similar ppt mixing ratio if the chloroacetic acid
19 calibration sensitivity is applied) exhibiting a near typical diurnal profile with ~~mixing ratios~~abundance rising
20 sharply after sunrise, at the same rate as the chlorine atom production but maintaining mixing ratios past noon
21 longer than that of isoprene and the chlorine atom.

22 The daily maxima of CMBO varied throughout the campaign and can be explained by the relative mixing ratios
23 of its precursors; the chlorine atom and isoprene. Its mixing ratio throughout the campaign followed similar
24 intensities to its precursors and figure 9 highlights its dependence on both Cl atom and isoprene mixing ratios. The
25 production rate of Cl and mixing ratio of isoprene were relatively low ~~from~~from the 24th to the 27th of May
26 (~~1.6x10⁵ x 10⁵~~ molecules cm⁻³ s⁻¹ Cl and 0.5 ppb isoprene), which resulted in relatively low CMBO mixing ratios.
27 An increase in isoprene and Cl on the 28th to the 30th May was subsequently mirrored by the CMBO levels as
28 qualitatively expected. On closer inspection of the 30th and 31st May, the mixing ratio of CMBO was lower than
29 expected on the 30th due to higher chlorine atom and isoprene mixing ratios compared ~~to~~with the ~~31st~~31st. This
30 could be explained by anticipated higher OH mixing ratio as calculated by the steady state model, which is also
31 further represented by higher mixing ratios of IEPOX (isoprene epoxydiols, i.e. OH oxidation products) on the
32 30th. This illustrates how the ToF-CIMS can identify isoprene oxidation products of two competing oxidation
33 pathways. The high levels of IEPOX on the 28th May can also possibly describe the relatively high levels of CMBO
34 in the particle phase due to an already well oxidised air mass. CMBO may also not be unique to only isoprene-
35 chloride reactions and therefore have alternative sources not represented in this data set.

36 Further daily oxidation rates can be probed via analysis of the related isoprene oxidation products observed by the
37 CIMS. Figure 10 depicts the diurnal time series of the precursor itself and several Cl-VOC products and IEPOX.

1 CMBO mixing ratios rise rapidly after sunrise due to the low mixing ratio of OH and high production rate of the
2 chlorine atom. The secondary and tertiary products, C₅H₉ClO₂ and C₅H₉ClO₃ (also measured in the laboratory by
3 Wang *et al.*, 2017) increased in mixing ratio at a much slower rate, but appear to peak later in the day (4 pm)
4 whereas CMBO peaked around 10 am (similar to the ClNO₂ peak time) and fall off, due to its further oxidation to
5 form the secondary and tertiary products. IEPOX mixing ratios increased slowly after sunrise and peaked later in
6 the day, as expected due to the availability of OH and competition from the chlorine atom chemistry. The similar
7 time series of the secondary and tertiary products to IEPOX was also reported by Wang *et al.*, (2017) and were
8 suggested to be ideal tracers of SOA production.

9

10 3.6.2 Anthropogenic Cl-VOC production

11 A similar unique chlorine oxidation marker in urban coastal areas, has been reported in the literature for 1, 3
12 butadiene; 4-chlorocrotonaldehyde (CCA) (Wang *et al.*, 2000). No measurements of 1, 3 butadiene were made
13 during this field campaign, although due to its common source to benzene (automobile exhausts (Ye *et al.*, 1998),
14 we present a comparison of the CCA measured by CIMS and benzene measurements made by the PTR-MS. The
15 intensity of CCA in both the gas and particle phase ~~with mixing ratio in the gas phase up to 13 ppt~~ reflect well the
16 ~~mixing ratios~~ abundance of its precursors. The maximum mixing ratio of the chlorine atom coincides with a high
17 mixing ratio of benzene and subsequently CCA on the 30th May whereas very low levels of CCA were observed
18 for the beginning of the campaign (Figure 11).

19 The diurnal time series of benzene (Figure 12) indicates high mixing ratios in the early hours of the day, possibly
20 associated with high anthropogenic activity or an inflow of urban air masses from downtown Beijing. The mixing
21 ratio falls off throughout the day and almost perfectly anti correlates with the CCA gas phase diurnal profile which
22 increases from sunrise and peaks at 3 pm. The particle phase CCA diurnal time series steadily builds up throughout
23 the day and ~~does~~ not peak until late in the evening, providing evidence of SOA production from the chlorine
24 oxidation of anthropogenic pollutants.

25

26 4. Conclusions

27 A FIGAERO ToF-CIMS was utilised in Beijing to assess the liberation of chlorine atoms via inorganic halogen
28 photolysis. A suite of inorganic halogens were detected, namely ClNO₂ reaching mixing ratios up to 2900 ppt,
29 which is suggested to have an anthropogenic origin due to the particulate chlorine correlation with SO₂, benzene
30 and CO. ClNO₂ was identified in the particle phase at higher ratios with respect to its gas phase component than
31 expected, which may only prove to be significant at such elevated mixing ratios as observed in East Asia. ClNO₂
32 mixing ratios above LOD persisted up to 7 hours past sunrise, attributed to the lifetime of ClNO₂ at these high
33 mixing ratios and a possible in-flow of heavily polluted air masses from the downtown urban area. Supporting Cl₂
34 and HCl mixing ratios proved to be significant contributors to chlorine atom production via steady state
35 calculations ~~enabling an average daytime peak mixing ratio of chlorine atoms of 1.6 x10⁵ molecules cm⁻³.~~

1 Compared with data attained from European based campaigns, these mixing ratios exceed marine and urban
2 environments by at least an order of magnitude.

3 This high mixing ratio of chlorine atoms resulted in a steady state calculated OH:Cl ratios down to a factor of 6,
4 ~~enabling~~ suggesting Cl chemistry may be able to not only dominate alkane oxidation until midday but contribute
5 significantly to alkene oxidation throughout the day (15% on average). This enabled significant mixing ratios of
6 Cl-VOCs to be formed providing the first ambient high time resolution measurements of specific Cl-VOC species
7 simultaneously measured in the gas and particle phase. The measured unique markers of chlorine chemistry for
8 both biogenic and anthropogenic precursors provides quantitative and qualitative data to probe the extent of
9 chlorine atom chemistry and how they compete with OH. Simultaneous measurements of the VOC precursors via
10 PTR-MS, and IEPOX, Cl-VOCs with the CIMS provides rich information on SOA formation pathways via both
11 OH and chlorine atom oxidation. Multistep oxidation products of Cl-VOCs were also identified and can provide
12 partitioning information and SOA formation rates and lifetimes.

13 The results highlight deficiency in chlorine atom chemistry descriptions within models possibly due to a lack in
14 quantification and identification of Cl-VOC products in gas and particle phase. This work provides instrumental
15 capability to probe the competition between OH and Cl oxidation chemistry and quantify their effect on ozone and
16 SOA formation.

17 **Acknowledgement:**

18 The work was ~~done~~ carried out under the framework research program on ‘Photochemical smog in China’ financed
19 by Swedish Research Council (639-2013-6917). The National Natural Science Foundation of China (21677002)
20 and the National Key Research and Development Program of China (2016YFC0202003) also helped fund this
21 work.

23 **References**

- 24 Allan, W., Struthers, H. and Lowe, D. C.: Methane carbon isotope effects caused by atomic chlorine in the marine
25 boundary layer: Global model results compared with southern hemisphere measurements. *J. Geophys. Res.* 112,
26 2007.
- 27 AQIRP, 1995, Effects of gasoline T50, T90 and sulfur on exhaust emissions of current and future technology
28 vehicles. Auto/Oil Air Quality Improvement Research Program, Technical Bulletin No. 18.
- 29 Baker, A. K., Sauvage, C., Thorenz, U. R., van Velthoven, P., Oram, D. E., Zahn, A., Berninkmeijer, C. A. M.
30 and Williams, J.: Evidence for strong, widespread chlorine atom chemistry associated with pollution outflow
31 from continental Asia, *Sci. Rep.*, 6, 36821, 2016.
- 32 Bannan, T. J., Booth, A. M., Bacak, A., Muller, J. B. A., Leather, K. E., Le Breton, M., Jones, B., Young, D., Coe,
33 H., Allan, J., Visser, S., Slowik, J. G., Furger, M., Prevot, A. S. H., Lee, J., Dunmore, R. E., Hopkins, J. R.,
34 Hamilton, J. F., Lewis, A. C., Whalley, L. K., Sharp, T., Stone, D., Heard, D. E., Fleming, Z. L., Leigh, R.,
35 Shallcross, D. E., and Percival, C. J.: The first UK measurements of nitryl chlorine using a chemical ionization
36 mass spectrometer in central London in the summer of 2012, and an investigation of the role of Cl atom oxidation,
37 *J. Geophys. Res. Atmos.*, 120, 5638–5657, 2015.

- 1 Bannan, T. J., Bacak, A., Le Breton, M., Ouyang, B., Flynn, M., McLeod, M., Jones, R., Malkin, T. L., Whalley,
2 L. K., Heard, D. E., Bandy, B., Khan, A., Shallcross, D. E., and Percival, C. J.: Ground and airborne U.K.
3 measurements of nitryl chloride, an investigation of the role of Cl atom oxidation at Weybourne Atmospheric
4 Observatory, *J. Geophys. Res. Atmospheres*, 10.2017.
- 5 Brown, S. S. & Stutz, J. Nighttime radical observations and chemistry *Chem. Soc. Rev.*, The Royal Society of
6 Chemistry, 41, 6405-6447, 2012.
- 7 Burkholder, J.B. et al. *Chemical Kinetics and Photochemical Data for Use in Atmospheric Studies: Evaluation*
8 *Number 18*. Jet Propulsion Laboratory, California Institute of Technology, Pasadena, CA, 2015.
- 9 Cai, X., Ziemba, L. D. and Griffin, R. J.: Secondary aerosol formation from the oxidation of toluene by chlorine
10 atoms, *Atmos. Environ.*, 42, 32, 2008.
- 11 Brown, S. S., Stark, H., and Ravishankara, A. R.: Applicability of the steady state approximation to the
12 interpretation of atmospheric observations of NO₃ and N₂O₅, *J. Geophys. Res.- Atmos.*, 108, 4539, 2003.
- 13 Brown, S. S., Dube, W. P., Tham, Y. J., Zha, Q. Z., Xue, L. K., Poon, S., Wang, Z., Blake, D. R., Tsui, W., Parrish,
14 D. D., Wang, T.: Nighttime chemistry at a high altitude site above Hong Kong, *J. Geophys. Res. Atmos.*, Vol. 121,
15 Issue. 5, 2457-2475, 2016.
- 16
17 DeCarlo, P. F., Kimmel, J., Trimborn, A., Northway, M., Jayne, J. T., Aiken, A., Gonin, M., Fuhrer, K., Horvath,
18 T., Docherty, K., Worsnop, D. R., and Jimenez, J. L.: Field-deployable, high-resolution, time-of-flight Aerosol
19 Mass Spectrometer, *Anal. Chem.*, 78, 8281–8289, 2006.
- 20 de Gouw, J. and Warneke, C.: Measurements of volatile organic compounds in the earth's atmosphere using
21 proton-transferreaction mass spectrometry, *Mass Spectrom. Rev.*, 26, 223–257, 2007.
- 22 Faxon, C. B., Bean, J. K., and Ruiz, L. H.: Inland Mixing ratios of Cl₂ and ClNO₂ in Southeast Texas suggest
23 chlorine chemistry significantly contributes to atmospheric reactivity, *Atmosphere*, 6, 1487–1506, 2015.
- 24 Finley, B. D. and Saltzman, E. S: Measurement of Cl₂ in coastal urban air, *Geophys. Res. Lett.*, 33, 2006.
- 25 Fraser, M. P., G. R. Cass, B. R. Simoneit, & R. A. Rasmussen (1997). Air quality model evaluation data for
26 organics. 4. C₂-C₃₆ non-aromatic hydrocarbons. *Environmental science & technology*, 31(8), 2356-2367
27 DOI: 10.1021/es960980g
- 28 Hoffman, R. C., Gebel, M. E., Fox, B. S., and Finlayson-Pitts, B. J.: Knudsen cell studies of the reactions of
29 N₂O₅ and ClONO₂ with NaCl: Development and application of a model for estimating available surface areas and
30 corrected uptake coefficients, *Phys. Chem. Chem. Phys.*, 5, 9, 1780–1789, 2003.
- 31 Hofzumahaus, Andreas, Franz Rohrer, Keding Lu, Birger Bohn, Theo Brauers, Chih-Chung Chang, Hendrik
32 Fuchs, et al. "Amplified Trace Gas Removal in the Troposphere." *Science* 324, no. 5935 (2009): 1702.
- 33 Hu, W. W., Hu, M., Yuan, B., Jimenez, J. L., Tang, Q., Peng, J. F., Hu, W., Shao, M., Wang, M., Zeng, L. 74 M.,
34 Wu, Y. S., Gong, Z. H., Huang, X. F., and He, L. Y.: Insights on organic aerosol aging and the influence of
35 coal combustion at a regional receptor site of central eastern China, *Atmos. Chem. Phys.*, 76 13, 10095-10112,
36 2013.
- 37 Hu, W., Hu, M., Hu, W., Jimenez, J. L., Yuan, B., Chen, W., Wang M., We, Y., Chen, C., Wang, Z., Peng, J.,
38 Zeng, L. and Shao, M. Chemical composition, sources, and aging process of submicron aerosols in Beijing:
39 Contrast between summer and winter, *J. Geophys. Res.*, 121, 4, 1955-1977, 2016.
- 40 Huang, M., Liu, X., Hu, C., Guo, X., Gu, X., Zhao, W., Wang, Z., Fang, L. and Zhang, W.: Aerosol laser time-of-
41 flight mass spectrometer for the on-line measurement of secondary organic aerosol in smog chamber, *Meas. J. Int.*
42 *Meas. Confed.*, 55(3), 394–401, 2014.

- 1 Keil, A. and Shepson, P.: Chlorine and bromine atom ratios in the springtime Arctic troposphere as determined
2 from measurements of halogenated volatile organic compounds, *J. Geophys. Res.*, 111, 2006.
- 3 Kaiser, J. W., Heil, A., Andreae, M. O., Benedetti, A., Chubarova, N., Jones, L., Morcrette, J.-J., Razinger, M.,
4 Schultz, M. G., Suttie, M., and van der Werf, G. R. (2012). Biomass burning emissions estimated with a global
5 fire assimilation system based on observed fire radiative power. *Biogeosciences*, 9:527-554.
- 6 Kercher, J. P., Riedel, T. P., and Thornton, J. A.: Chlorine activation by N₂O₅: simultaneous, in situ detection of
7 ClNO₂ and N₂O₅ by chemical ionization mass spectrometry, *Atmos. Meas. Tech.*, 2, 193–204, doi:10.5194/amt-
8 2-193-2009, 2009.
- 9 Khan, M. A. H., Ashfold, M. J., Nickless, G., Martin, D., Watson, L. A., Hamer, P. D., Wayne, R. P., Canosa-
10 Mas, C. E. and Shallcross, D. E.: Night-time NO₃ and OH radical mixing ratios in the United Kingdom inferred
11 from hydrocarbon measurements, *Atmos. Sci. Lett.*, 9, 3, 140-146, 2008.
- 12 Kim, M. J., Farmer, D. K. and Bertram, T. H.: A controlling role for the air–sea interface in the chemical
13 processing of reactive nitrogen in the coastal marine boundary layer, *PNAS*, 111 (11), 2943-3948, 2014.
14
- 15 Lopez-Hilfiker, F. D., Mohr, C., Ehn, M., Rubach, F., Kleist, E., Wildt, J., Mentel, Th. F., Lutz, A., Hallquist, M.,
16 Worsnop, D., and Thornton, J. A.: A novel method for online analysis of gas and particle composition: description
17 and evaluation of a Filter Inlet for Gases and AEROSols (FIGAERO), *Atmos. Meas. Tech.* 2014, 7, 983–1001,
18 doi:10.5194/amt-7-983-2014.
- 19 Le Breton, M, Bannan, T. J., Shallcross, D. E., Khan, M. A., Evans, M. J., Lee, J., Lidster, R., Andrews, S.,
20 Carpenter, L., Schmidt, J., Jacob, D., Harris, N. R. P., Bauguutte, S.-J., Gallagher, M., Bacak, A., Leather, K. E.
21 and Percival, C. J.: Enhanced ozone loss by active inorganic bromine chemistry in the tropical troposphere, *Atmos.*
22 *Environ.*, 155, 21-28, 2017a.
- 23 Le Breton, M., Wang, Y., Hallquist, Å. M., Pathak, R. K., Zheng, J., Yang, Y., Shang, D., Glasius, M., Bannan,
24 T. J., Liu, Q., Chan, C. K., Percival, C. J., Zhu, W., Lou, S., Topping, D., Wang, Y., Yu, J., Lu, K., Guo, S., Hu,
25 M., and Hallquist, M.: Online gas and particle phase measurements of organosulfates, organosulfonates and
26 nitrooxyorganosulfates in Beijing utilizing a FIGAERO ToF-CIMS, *Atmos. Chem. Phys. Discuss.*,
27 <https://doi.org/10.5194/acp-2017-814>, in review, 2017b.
- 28 [Liu, Y., Yuan, B., Li, X., Shao, M., Lu, S., Li, Y., Chang, C.-C., Wang, Z., Hu, W., Huang, X., He, L., Zeng, L.,](#)
29 [Hu, M., and Zhu, T.: Impact of pollution controls in Beijing on atmospheric oxygenated volatile organic](#)
30 [compounds \(OVOCs\) during the 2008 Olympic Games: observation and modeling implications, *Atmos. Chem.*](#)
31 [Phys.](#), 15, 3045-3062, <https://doi.org/10.5194/acp-15-3045-2015>, 2015.
- 32 [Liu, J., D’Ambro, E. L., Lee, B. H., Lopez-Hilfiker, F., Zaveri, R. A., RiveraRios, J. C., Keutsch, F. N., Lyer, S.,](#)
33 [Kurtne, T., Zhang, Z., Gold, A., Surratt, J. D., Shilling, J. E. and Thornton, J. A.: Efficient Isoprene Secondary](#)
34 [Organic Aerosol Formation from a Non-IEPOX Pathway, *Environ. Sci. Technol.*, 50, 18, 9872-9880, 2016.](#)
- 35 Lopez-Hilfiker, F. D., Mohr, C., Ehn, M., Rubach, F., Kleist, E., Wildt, J., Mentel, Th. F., Lutz, A., Hallquist, M.,
36 Worsnop, D., and Thornton, J. A.: A novel method for online analysis of gas and particle composition: description
37 and evaluation of a Filter Inlet for Gases and AEROSols (FIGAERO), *Atmos. Meas. Tech.* 2014, 7, 983–1001,
38 doi:10.5194/amt-7-983-2014.
- 39 Ma, Q., Shuxiao, S. C., Zhao, B., Martin, R. V., Brauer, M., Cohen, A., Jiang, J., Zhou, W., Hao, J., Frostad, J.,
40 Forouzanfar, M. H. and Burnett, T.: Impacts of coal burning on ambient PM₁ pollution in China, *Atmos. Chem.*
41 *Phys.*, 17, 4477-4491, 2017.
- 42 Manion, J. A., R. E. Huie, R. D. Levin, D. R. Burgess Jr, V. L Orkin, W. Tsang, W. S. McGivern, J. W. Hudgens,
43 V. D. Knyazev, D. B Atkinson, E. Chai, A. M. Tereza, C.-Y. Lin, T. C. Allison, W. G. Mallard, F. Westley, J.
44 T. Herron, R. F. Hampson, and D. H. Frizzell (2014) NIST Chemical Kinetics Database, NIST Standard Reference

1 Database 17, Version 7.0 (Web Version), Release 1.6.8, Data version 2013.03, National Institute of Standards and
2 Technology, Gaithersburg, Maryland, 20899-8320. Web address: <http://kinetics.nist.gov/>

3 Mielke, L. H., Furgeson, A., Odam-Ankrah, C. A., and Osthoff, H. D.: Ubiquity of ClNO₂ in the urban boundary
4 layer of Calgary, AB, Canada, *Canadian J. Chem.*, 2015.

5 Nordmeyer, T., Wang, W., Ragains, M. L., Finlayson-Pitts, B. J., Spicer, C. W. and Plastridge, R. A.: Unique
6 products of the reaction of isoprene with atomic chlorine: Potential markers of chlorine atom chemistry, *Geophys.*
7 *Res. Lett.*, 24(13), 1615–1618, doi:10.1029/97GL01547, 1997.

8 Ofner, J., Balzer, N., Buxmann, J., Grothe, H., Schmitt-Kopplin, P., Platt, U. and Zetzsch, C.: Halogenation
9 processes of secondary organic aerosol and implications on halogen release mechanisms, *Atmos. Chem. Phys.*,
10 12(13), 5787–5806, doi:10.5194/acp-12-5787-2012, 2012.

11 Orlando, J. J., Tyndall, G. S., Apel, E. C., Riemer, D., and Paulson, S. E.: Rate coefficients and mechanisms of the
12 reaction of Cl-atoms with a series of unsaturated hydrocarbons under atmospheric conditions, *Int. J. Chem. Kinet.*,
13 35, 334–353, 2003.

14 Osthoff, H.D.; Roberts, J.M.; Ravishankara, a. R.; Williams, E.J.; Lerner, B.M.; Sommariva, R.; Bates, T.S.;
15 Coffman, D.; Quinn, P.K.; Dibb, J.E.: High levels of nitryl chlorine in the polluted subtropical marine boundary
16 layer. *Nat. Geosci.* 2008, 1, 324–328, 2008.

17 Platt, U., Allan, W., and Lowe, D.: Hemispheric average Cl atom mixing ratio from ¹³C/¹²C ratios in atmospheric
18 methane, *Atmos. Chem. Phys.*, 4, 2393–2399, 4, 2004.

19 Phillips, G. J., Tang, M. J., Thieser, J., Brickwedde, B., Schuster, G., Bohn, B., Lelieveld, J., and Crowley, J. N.:
20 Significant mixing ratios of nitryl chlorine observed in rural continental Europe associated with the influence of
21 sea salt chlorine and anthropogenic emissions, *Geophys. Res. Lett.*, 39, L10811, 2016.

22 Phillips, G. J., Thieser, J., Tang, M., Sobanski, N., Schuster, G., Fachinger, J., Drewnick, F., Borrmann, S.,
23 Bingemer, H., Lelieveld, J. and Crowley, J. N.: Estimating N₂O₅ uptake coefficients using ambient measurements
24 of NO₃, N₂O₅, ClNO₂ and particle-phase nitrate, *Atmos. Chem. Phys.*, 16, 13231-13249, 2016.

25 Pszenny, A. A. P., Fischer, E. V., Russo, R. S., Sive, B. C., and Varner, R. K.: Estimates of Cl atom mixing ratios
26 and hydrocarbon kinetic reactivity in surface air at Appledore Island, Maine (USA), during International
27 Consortium for Atmospheric Research on Transport and Transformation/Chemistry of Halogens at the Isles of
28 Shoals, *J. Geop*

29 Riedel, T. P., Bertram, T. H., Crisp, T. A., Williams, E. J., Lerner, B. M., Vlasenko, A., Li, S. M., Gilman, J., de
30 Gouw, J., Bon, D. M., Wagner, N. L., Brown, S. S., and Thornton, J. A.: Nitryl chlorine and molecular chlorine in
31 the coastal marine boundary layer, *Environ. Sci. Technol.*, 46, 10463–10470, 2012.

32 Riedel, T. P., Wolfe, G. M., Danas, K. T., Gilman, J. B., Kuster, W. C., Bon, D. M., Vlasenko, A., Li, S. M.,
33 Williams, E. J., Lerner, B. M., Veres, P. R., Robert, J. M., Holloway, J. S., Lefer, B., Brown, S.S. and Thornton,
34 J. A.: An MCM modeling study of nitryl chlorine (ClNO₂) impacts on oxidation, ozone production and nitrogen
35 oxide partitioning in polluted continental outflow, *Atmos. Chem. Phys.*, 14, 3789-3800, 2014.

36 Riemer, D. D., Apel, E. C., Orlando, J. J., Tyndall, G. S., Brune, W. H., Williams, E. J., Lonneman, W. A. and
37 Neece, J. D.: Unique isoprene oxidation products demonstrate chlorine atom chemistry occurs in the Houston,
38 Texas urban area, *J. Atmos. Chem.*, 61(3), 227–242, 2008.

39 Riva, M., Healy, R. M., Flaud, P. M., Perraudin, E., Wenger, J. C. and Villenave, E.: Gas- and Particle-Phase
40 Products from the Chlorine-Initiated Oxidation of Polycyclic Aromatic Hydrocarbons, *J. Phys. Chem. A*, 119(45),
41 11170–11181, doi:10.1021/acs.jpca.5b04610, 2015.

1 Roberts, J. M., Osthoff, H. D., Brown, S. S., and Ravishankara, A. R.: N₂O₅ oxidizes chloride to Cl₂ in acidic
2 atmospheric aerosol, *Science*, 321, 1059–1059, doi:10.1126/science.1158777, 2008.

3 Sander, R.: Modeling atmospheric chemistry: Interactions between gas-phase species and liquid cloud/aerosol
4 particles, *Surv. Geophys.*, 20, 1–31, 1999.

5 Sarwar, G., Simon, H., Xing, J., and Mathur, R.: Importance of tropospheric ClNO₂ chemistry across the Northern
6 Hemisphere, *Geophys. Res. Lett.*, 41, 4050–4058, 2014.

7 Simpson, D., Benedictow, A., Berge, H., Bergström, R., Emberson, L. D., Fagerli, H., Flechard, C. R., Hayman,
8 G. D., Gauss, M., Jonson, J. E., Jenkin, M. E., Nyíri, A., Richter, C., Semeena, V. S., Tsyro, S., Tuovinen, J.-P.,
9 Valdebenito, Á., and Wind, P.: The EMEP MSC-W chemical transport model – technical description, *Atmos.*
10 *Chem. Phys.*, 12, 7825-7865, <https://doi.org/10.5194/acp-12-7825-2012>, 2012.

11 Simon, H., Y. Kimura, G. McGaughy, D.T. Allen, S.S. Brown, H.D. Osthoff, J.M. Roberts, 422 D. Byun, and D.
12 Lee.: Modeling the impact of ClNO₂ on ozone formation in the 423 Houston area, *J. Geophys. Res.*, 114, D00F03,
13 424 doi:10.1029/2008JD010732, 2009.

14 Skamarock, W. C., J. B. Klemp, J. Dudhia, D. O. Gill, D. M. Barker, M. G Duda, X.-Y. Huang, W. Wang, and J.
15 G. Powers, 2008: A Description of the Advanced Research WRF Version 3. NCAR-Tech, 113,
16 doi:10.5065/D68S4MVH

17 Tanaka, P. L., Riemer, D. D., Chang, S., Yarwood, G., McDonaldBuller, E. C., Apel, E. C., Orlando, J. J., Silva,
18 P. J., Jimenez, J. L., Canagaratna, M. R., Neece, J. D., Mullins, C. B., and Allen, D. T.: Direct evidence for
19 chlorine-enhanced urban ozone formation in Houston, Texas, *Atmos. Environ.*, 37, 1393–1400, 2003.

20 Tham, Y., Yan, C., Xue, L., Zha, Q., Wang, X., and Wang, T.: Presence of high nitryl chlorine in Asian coastal
21 environment and its impact on atmospheric photochemistry, *China Sci. Bull.*, 59, 356–359, doi:10.1007/s11434-
22 013-0063-y, 2014.

23 Thornton, J. A., Kercher, J. P., Riedel, T. P., Wagner, N. L., Cozic, J., Holloway, J. S., Dube, W. P., Wolfe, G. M.,
24 Quinn, P. K., Middlebrook, A. M., Alexander, B., and Brown, S. S.: A large atomic chlorine source inferred from
25 mid-continental reactive nitrogen chemistry, *Nature*, 464, 271–274, doi:10.1038/nature08905, 2010.

26 Wagner, N. L., Riedel, T. P., Young, C. J., Bahreini, R., Brock, C. A., Dube, W. P., Kim, S., Middlebrook, A. M.,
27 Öztürk, F., Robert, J. M., Russo, R., Sive, B., Swarthout, R., Thornton, J. A., VandenBoer, T. C., Zhou, Y. and
28 Brown, S. S.: N₂O₅ uptake coefficients and nocturnal NO₂ removal rates determined from ambient wintertime
29 measurements, 118, 16, 9331-9350, 2013.

30 Wang, W. and Finlayson-Pits, B. J.: Unique markers of chlorine atom chemistry in coastal urban areas: The
31 reaction with 1,3-butadiene in air at room temperature, *J. Geophys. Res.*, 106, 5, 4939-4958, 2001.

32 Wang, T., Cheung, T., Li, Y., Yu, X. and Blake, D.: Emission characteristics of CO, NO_x, SO₂ and indications of
33 biomass burning observed at a rural site in eastern China. *J. Geophys. Res. Atmos.*, 107, 12, 2002.

34 Wang, T., Tham, Y.J., Xue, L., Li, Q., Zha, Q., Wang, Z., Poon, S.C.N., Dube, W.P., Blake, D.R., Louie, P.K.K.,
35 Luk, C.W.Y., Tsui, W., Brown, S.S.: Observations of nitryl chlorine and modeling its source and effect on ozone
36 in the planetary boundary layer of southern China. *J. Geophys. Res.* 121, 2476e2489, 2016

37 Wang, H., Chen, J. and Lu, K.: Development of a portable cavity-enhanced absorption spectrometer for the
38 measurement of ambient NO₃ and N₂O₅: experimental setup, lab characterizations, and field applications in a
39 polluted urban environment, *Atmos. Chem. Phys.*, 10, 1465-1479, 2017.

40 Wang, X., Wang, H., Xue, L., Wang, T., Wang, L., Gu, R., Wang, W., Than, Y. T., Wang, Z., Yang, L., Chen, J.
41 and Wang, W.: Observations of N₂O₅ and ClNO₂ at a polluted urban surface site in North China: High N₂O₅ uptake
42 coefficients and low ClNO₂ product yields, *Amtos. Environ.*, 156, 125-134, 2017.

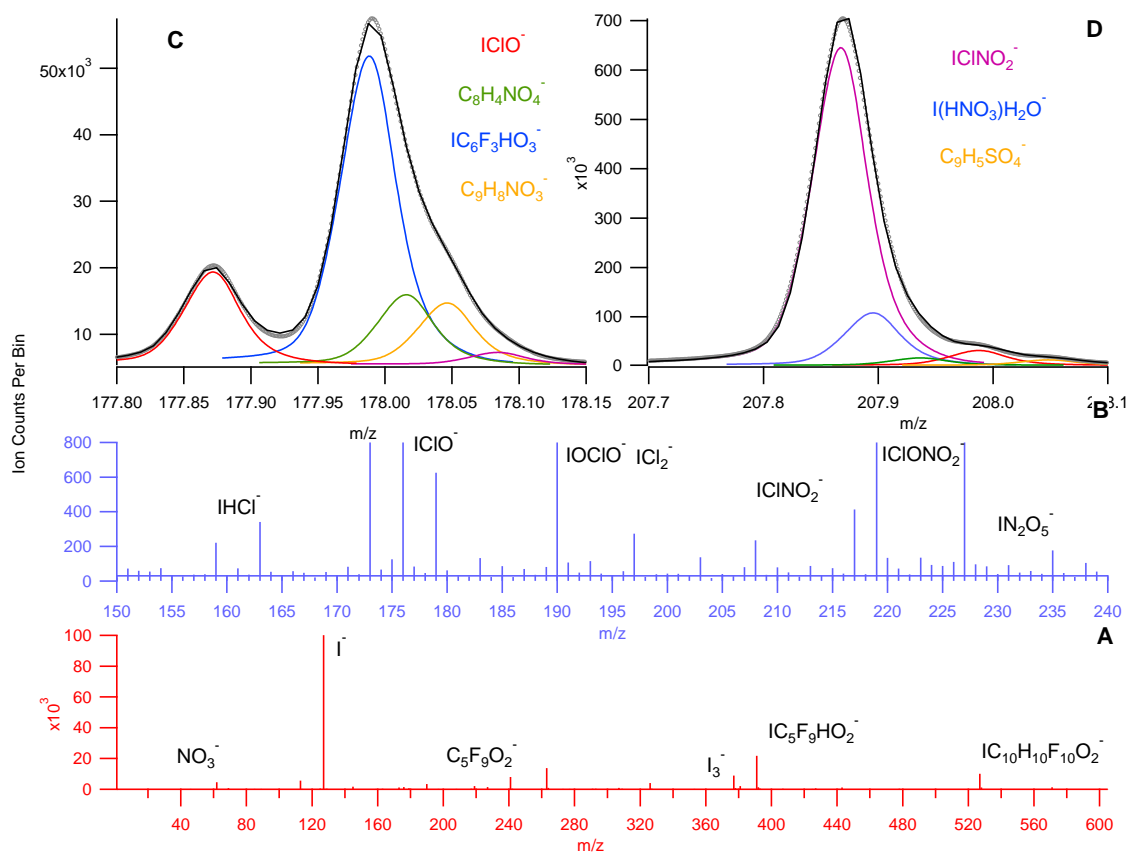
- 1 Wang, Z., Wang, W., Tham, Y. J., Hao, Q. L., Wang, L. W., Xinfeng., W., Wang, L. W. and Wang, T.: Fast
2 heterogeneous N₂O₅ uptake and ClNO₂ production in power plant plumes observed in the nocturnal residual layer
3 over the North China Plain, *Atmos. Chem. Phys. Discuss.*, 2017.
- 4 Wang, D. and Ruiz, L. H.: Secondary organic aerosol from chlorine-initiated oxidation of isoprene, *Atmos. Chem.*
5 *Phys. Discuss.*, 2017-342, 2017.
- 6 Whalley, L. K., Furneaux, K. L., Goddard, A., Lee, J. D., Mahajan, A., Oetjen, H., Read, K. A., Kaaden, N.,
7 Carpenter, L. J., Lewis, A. C., Plane, J. M. C., Saltzman, E. S., Wiedensohler, A., and Heard, D. E.: The chemistry
8 of OH and HO₂ radicals in the boundary layer over the tropical Atlantic Ocean, *Atmos. Chem. Phys.*, 10, 1555-
9 1576, <https://doi.org/10.5194/acp-10-1555-2010>, 2010.
- 10 Wiedinmyer, C., S. K. Akagi, R. J. Yokelson, L. K. Emmons, J. A. Al-Saadi, J. J. Orlando, and A. J. Soja. "The
11 Fire Inventory from Ncar (Finn): A High Resolution Global Model to Estimate the Emissions from Open Burning."
12 *Geoscientific Model Development* 4, no. 3 (2011): 625-41.
- 13 Ye, Y., Galbally, I. E., Weeks, I. A., Duffy, B. L., and Nelson, P. F.: Evaporative emissions of 1,3-butadiene from
14 petrol-fuelled motor vehicles, *Atmos. Environ.*, 32, 2685–2692, 1998.
- 15 Young, C. J., Washenfelder, R. A., Roberts, J. M., Mielke, L. H., Osthoff, H. D., Tsai, C., Pikelnaya, O., Stutz, J.,
16 Veres, P. R., Cochran, A. K., VandenBoer, T. C., Flynn, J., Grossberg, N., Haman, C. L., Lefer, B., Stark, H.,
17 Graus, M., de Gouw, J., Gilman, J. B., Kuster, W. C., and Brown, S. S.: Vertically Resolved Measurements of
18 Nighttime Radical Reservoirs; in Los Angeles and Their Contribution to the Urban Radical Budget, *Environ. Sci.*
19 *Technol.*, 46, 10965–10973, doi:10.1021/es302206a, 2012.
- 20
- 21 [Zou, Q., Lu, K. D., Wu, Y. S., Yang, Y. D., Du, Z. F., and Hu, M.: Ambient photolysis frequency of NO₂ deter-](#)
22 [ined using chemical actinometer and spectroradiometer at an urban site in Beijing, *Front Env Sci Eng*, 10, ARTN](#)
23 [13 10.1007/s11783-016-0885-3, 2016.](#)

24

25 **Table 1. Identified Cl-VOC reaction products, nomenclature of Cl-VOC and precursor compound.**

| CI-VOC | Potential nomenclature | Precursor |
|---|---------------------------------------|----------------|
| CHClO | formyl chloride | formaldehyde |
| C ₂ H ₃ ClO | chloroacetaldehyde | acetaldehyde |
| C ₃ H ₅ ClNO ₅ | Chloro PPN | PPN |
| C ₂ H ₃ ClNO ₅ | chloro PAN | PAN |
| C ₃ H ₅ ClO | chloroacetone | acetone |
| C ₂ H ₃ ClO ₂ | chloroacetic acid | acetic acid |
| CHClO ₂ | chloroformic acid | formic acid |
| C ₄ H ₇ ClO | chloro MEK or butanal | isoprene |
| C ₅ H ₆ ClO | CMBO - chloro 3-methyl-3-butene-2-one | isoprene |
| C ₅ H ₉ ClO ₂ | - | isoprene |
| C ₅ H ₉ ClO ₃ | - | isoprene |
| C ₃ H ₅ ClO | propanoyl chloride | 1, 3 butadiene |
| C ₈ H ₉ Cl | chloroethyl benzene | aromatic |

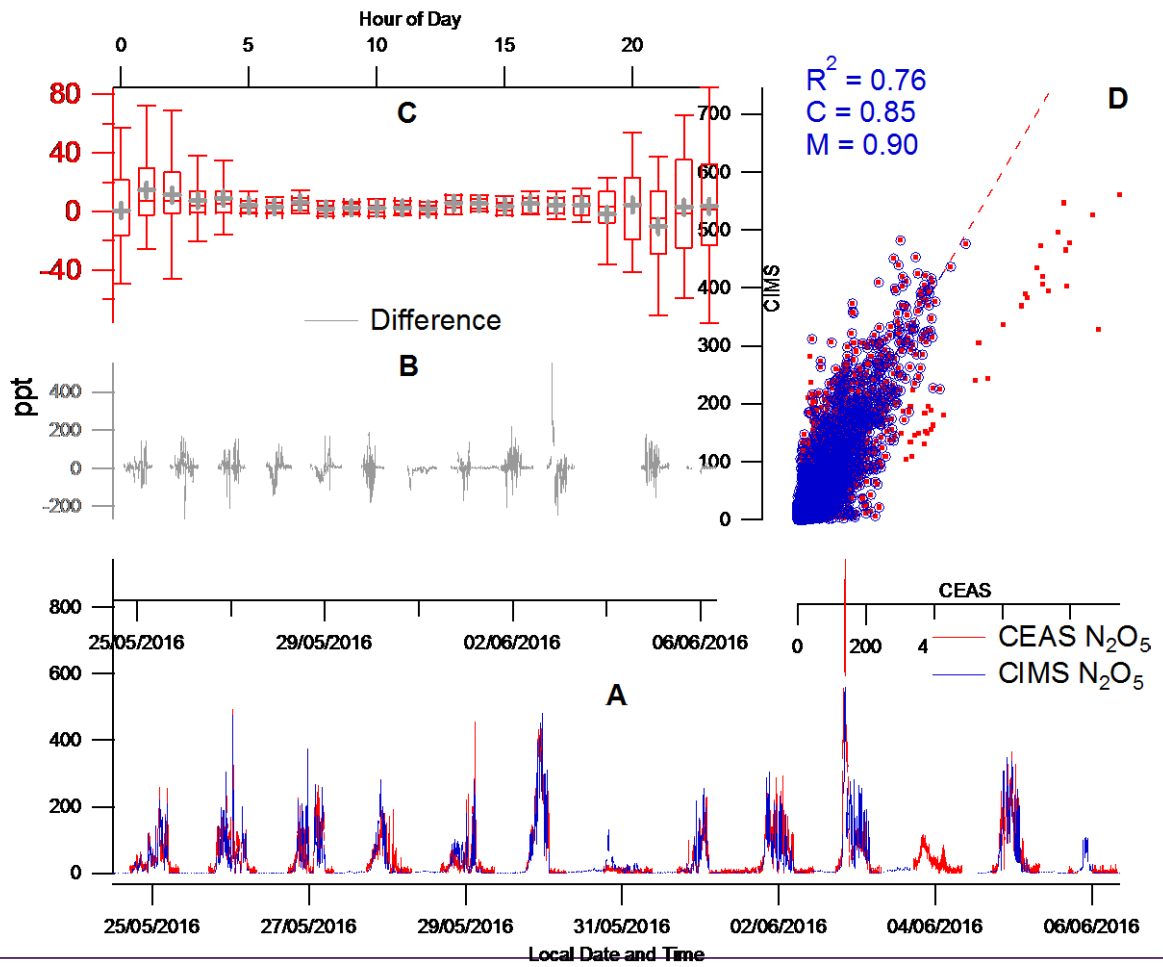
1
2
3



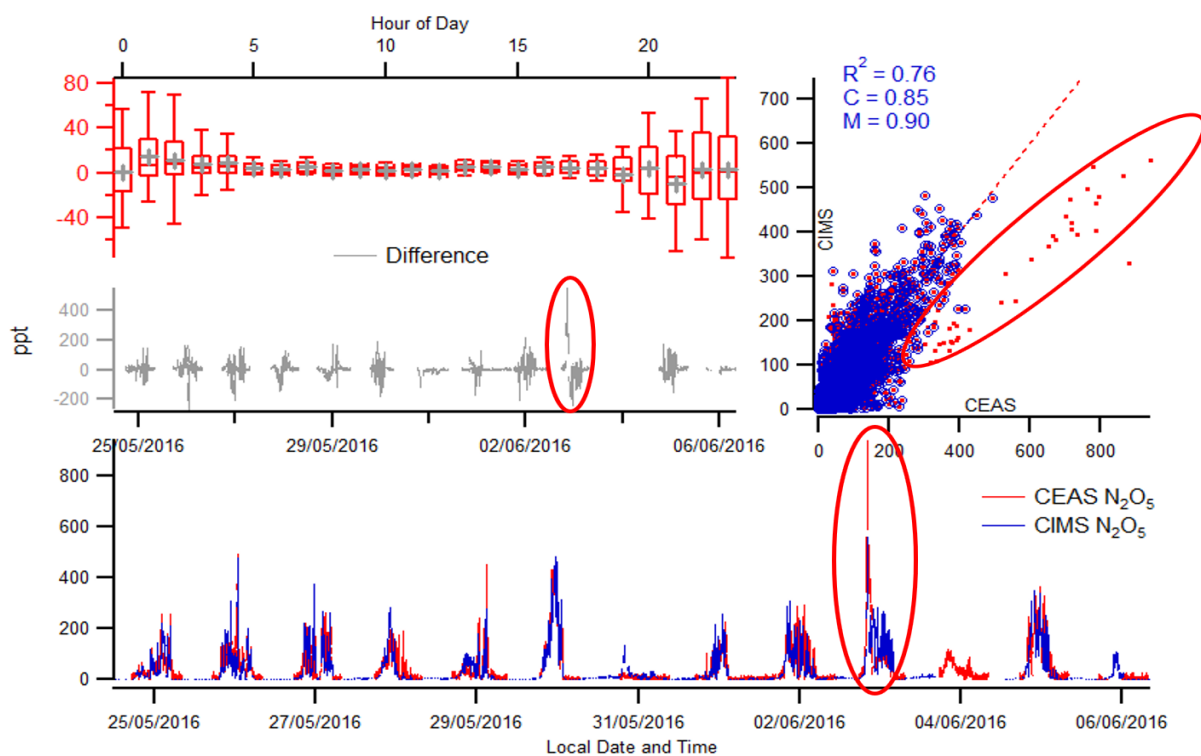
4

5 **Figure 1. Panel A: Average mass spectrum for the whole measured range. Panel B: Average mass spectrum**
6 **for the region that contains all gas phase night time species utilised in this work. A high resolution spectral**

- 1 fit for ClO and ClNO₂ are displayed with corresponding multi peaks with 0.5 AMU (panels C and D). The
- 2 black line represents the total fit from all peaks. The grey line represents the mass spectral raw data.



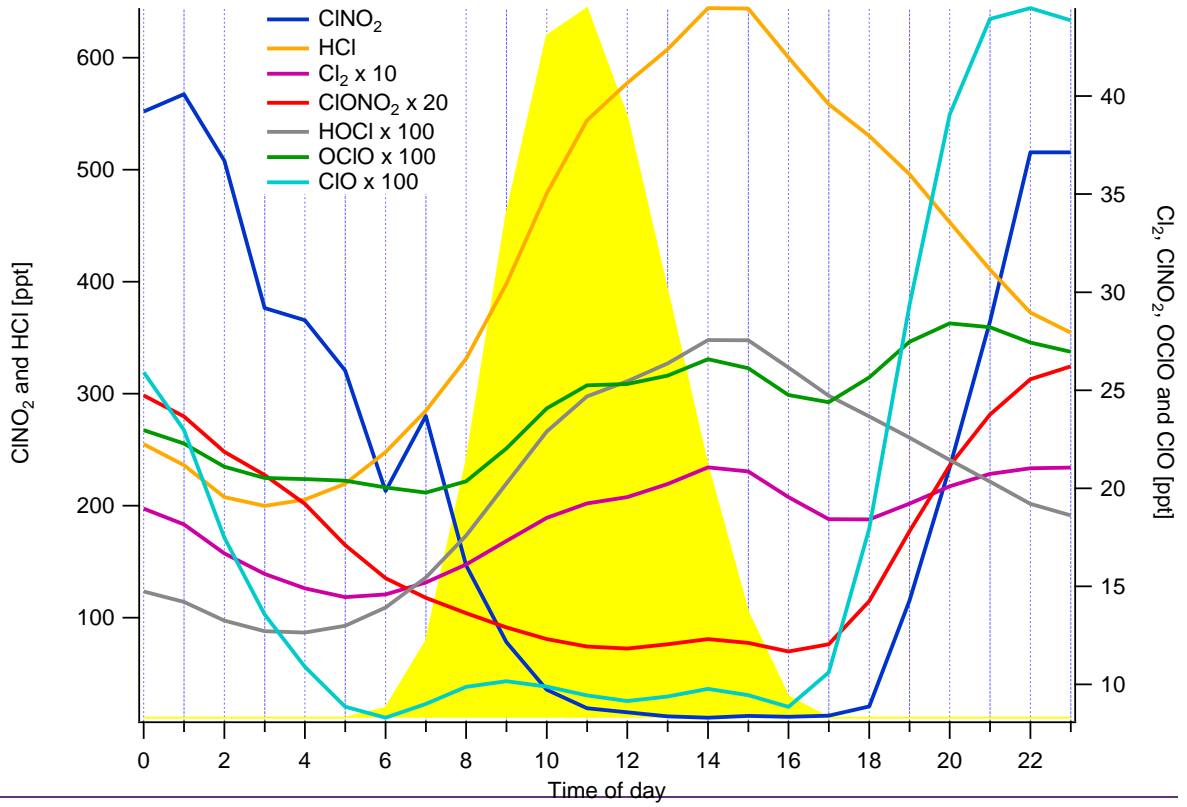
3



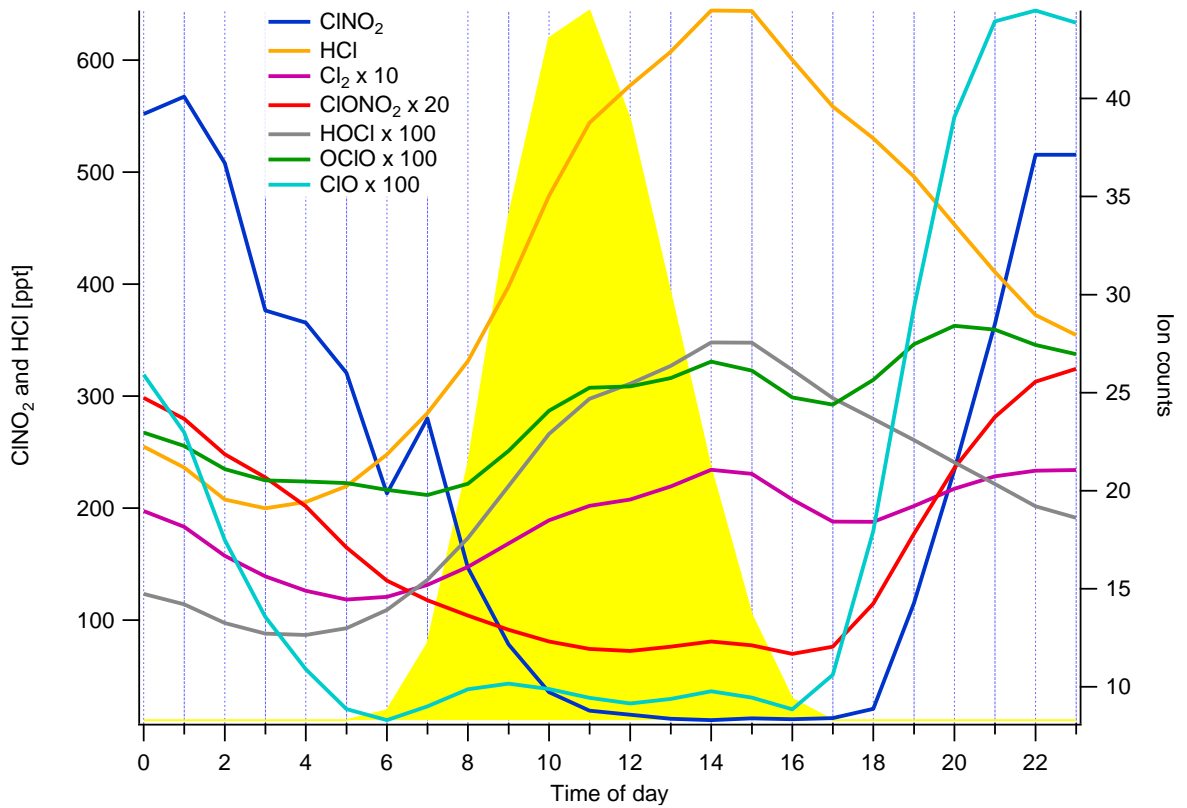
1

2 **Figure 2. CIMS and CEAS one minute averaged data of N₂O₅ with corresponding correlation plot (panel**
 3 **A), campaign and diurnal deviation (panels B and C respectively). The red highlighted periods represent**
 4 **data collected on the 3rd June where a different correlation gradient was observed between CIMS and**
 5 **CEAS. The box and whisker plot represents the diurnal difference for the campaign between the CEAS and**
 6 **CIMS measurements (panel D). C is the y-intercept of the line of best fit and M is the gradient.**

7



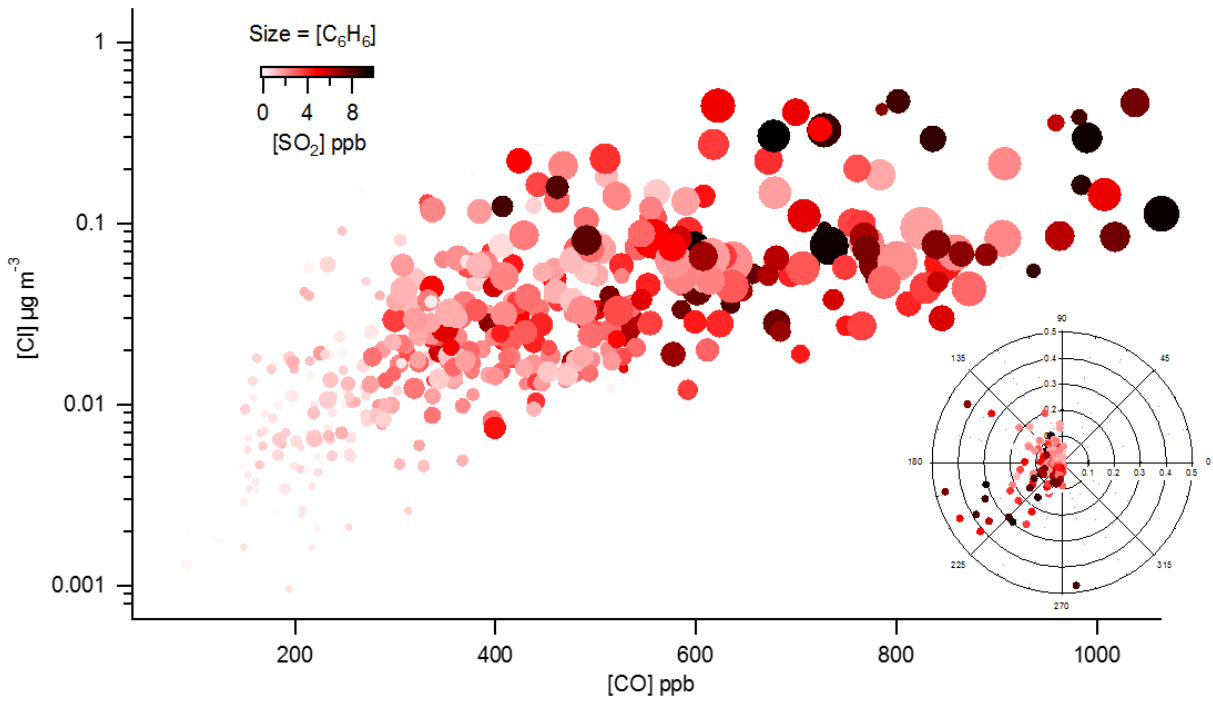
1



2

3 **Figure 3. Mean diurnal profiles of the inorganic halogens detected by the CIMS from the 23rd May to 6th**
 4 **June with average J rate for ClNO₂ as guide for photolysis. ClNO₂ and HCl mixing ratios are on the left y-**
 5 **axis and the other inorganic halogens on the right y-axis displayed in ion counts.**

1



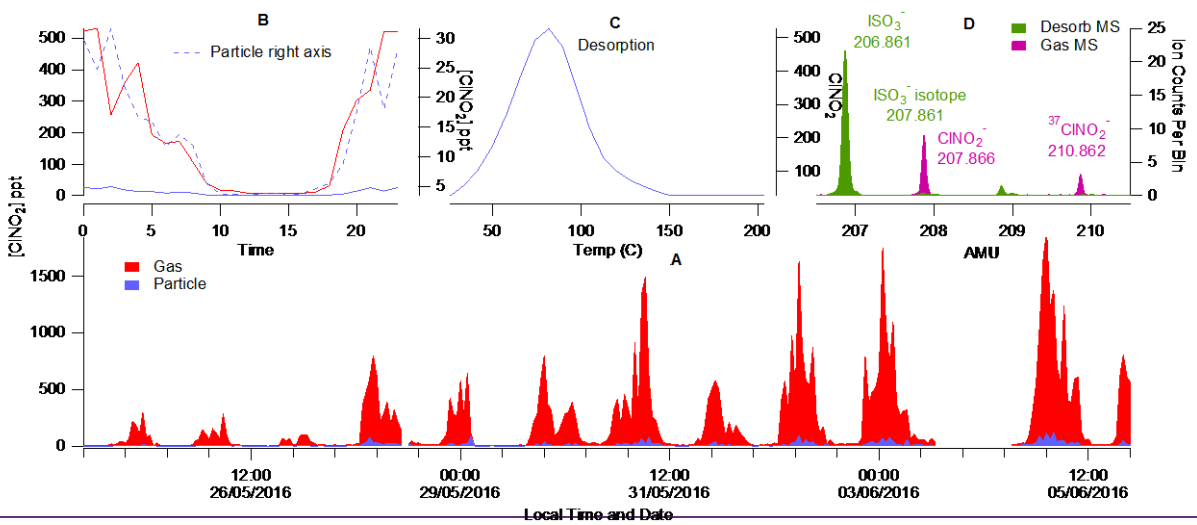
2

3 **Figure 4. Correlation of particulate Cl⁻ from the AMS measurements and CO colour coded by SO₂ mixing**
 4 **ratio and size binned by increasing benzene mixing ratio. A wind rose plot illustrates the wind direction and**
 5 **particulate Cl⁻ mixing ratio colour coded by SO₂ mixing ratio.**

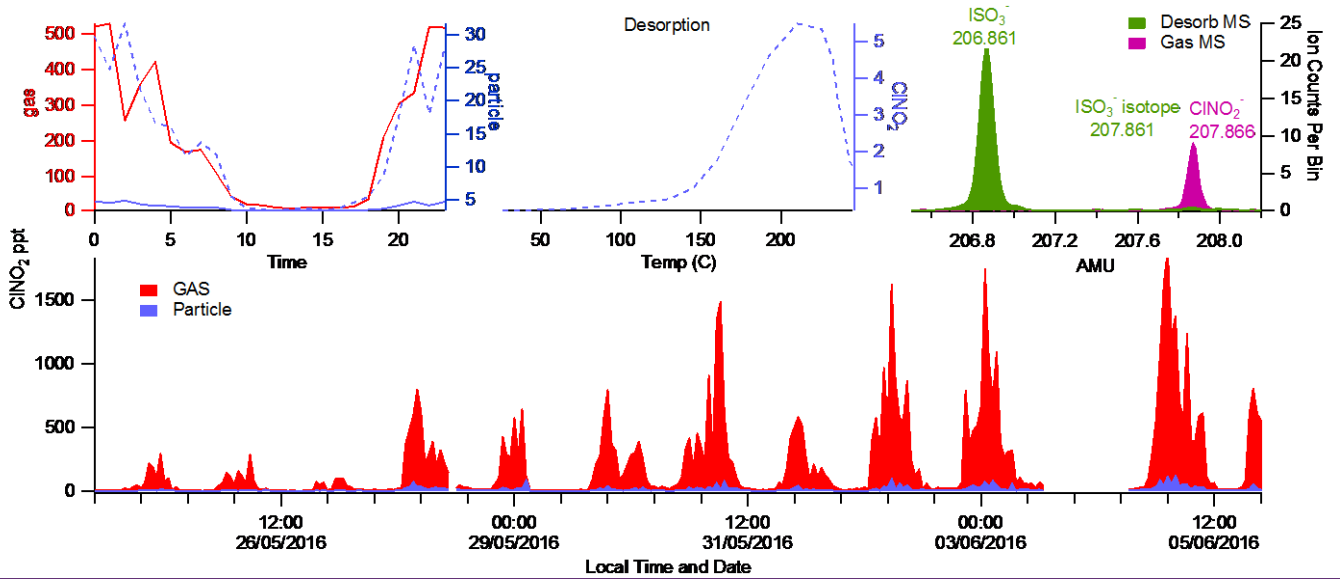
6

7

8



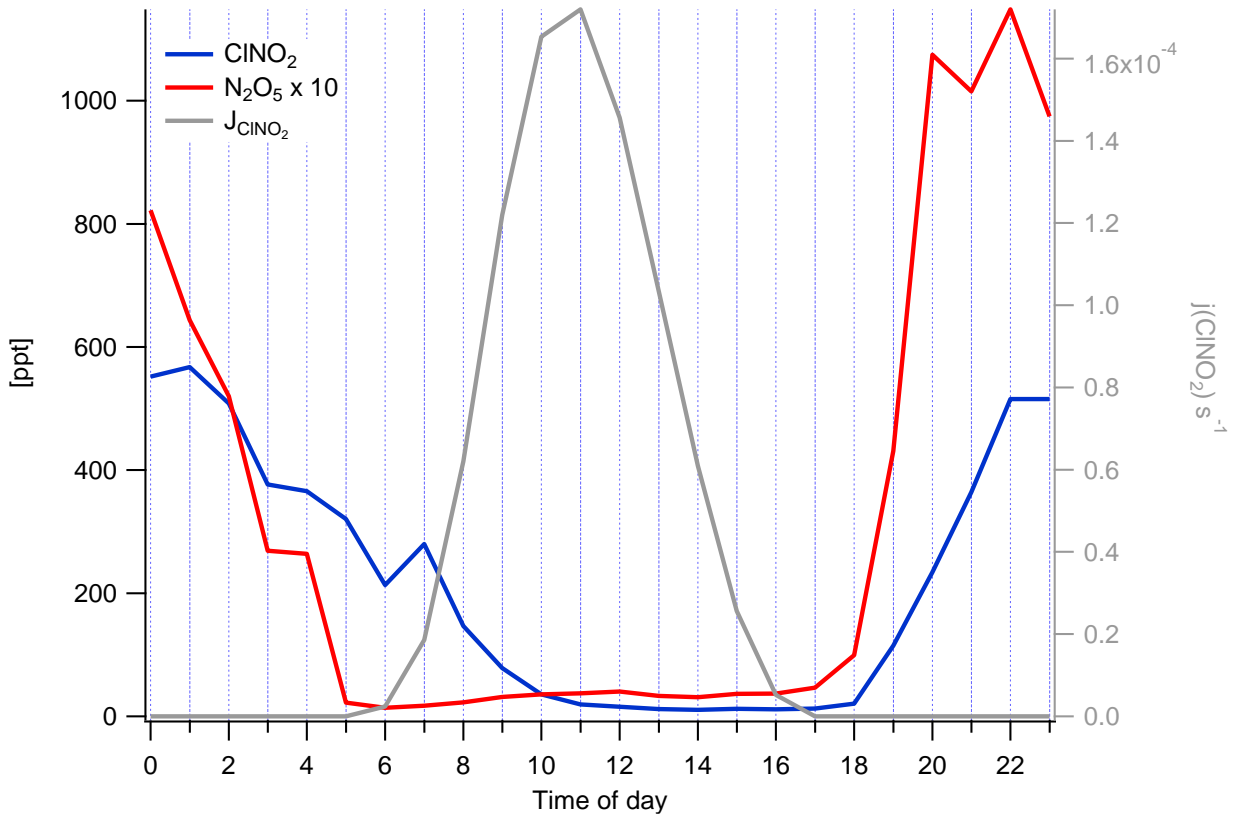
9



1

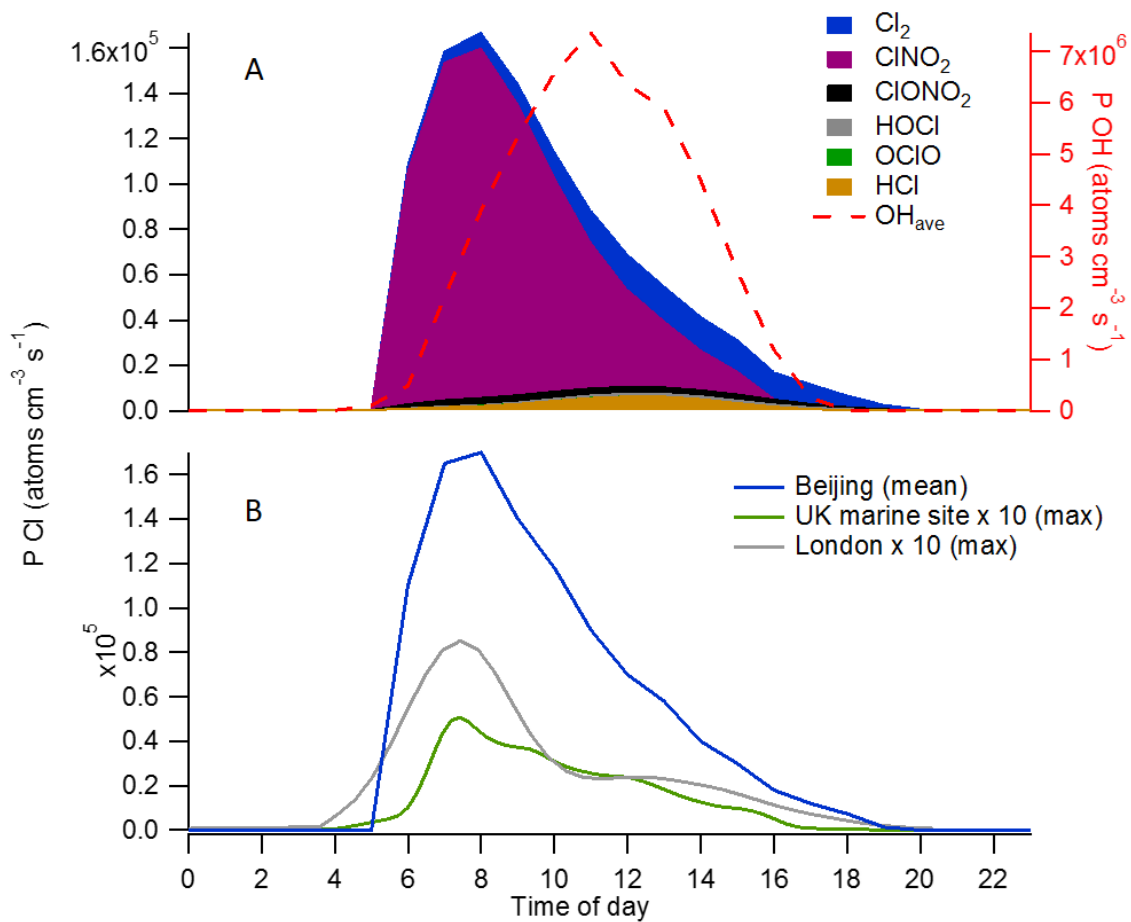
2 **Figure 5. CINO₂ gas and particle phase campaign time series (1 hour averaged) (panel A) and average**
 3 **diurnal profiles Panel B). The peak fitting for CINO₂ and the SO₃ interfering mass at 207-208 AMU (panel**
 4 **C) and the desorption profile for the counts attributed to the high resolution CINO₂ peak (panel D).**

5



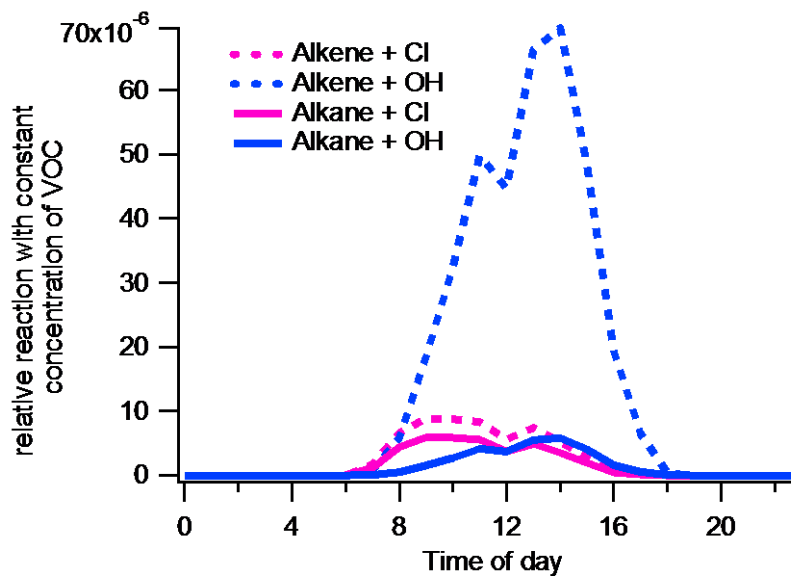
6

7 **Figure 6. Diurnal profile of N₂O₅, CINO₂ and j(CINO₂) for the campaign highlighting the persistence of**
 8 **CINO₂ passed sunrise and the expected rapid photolysis of N₂O₅.**



1

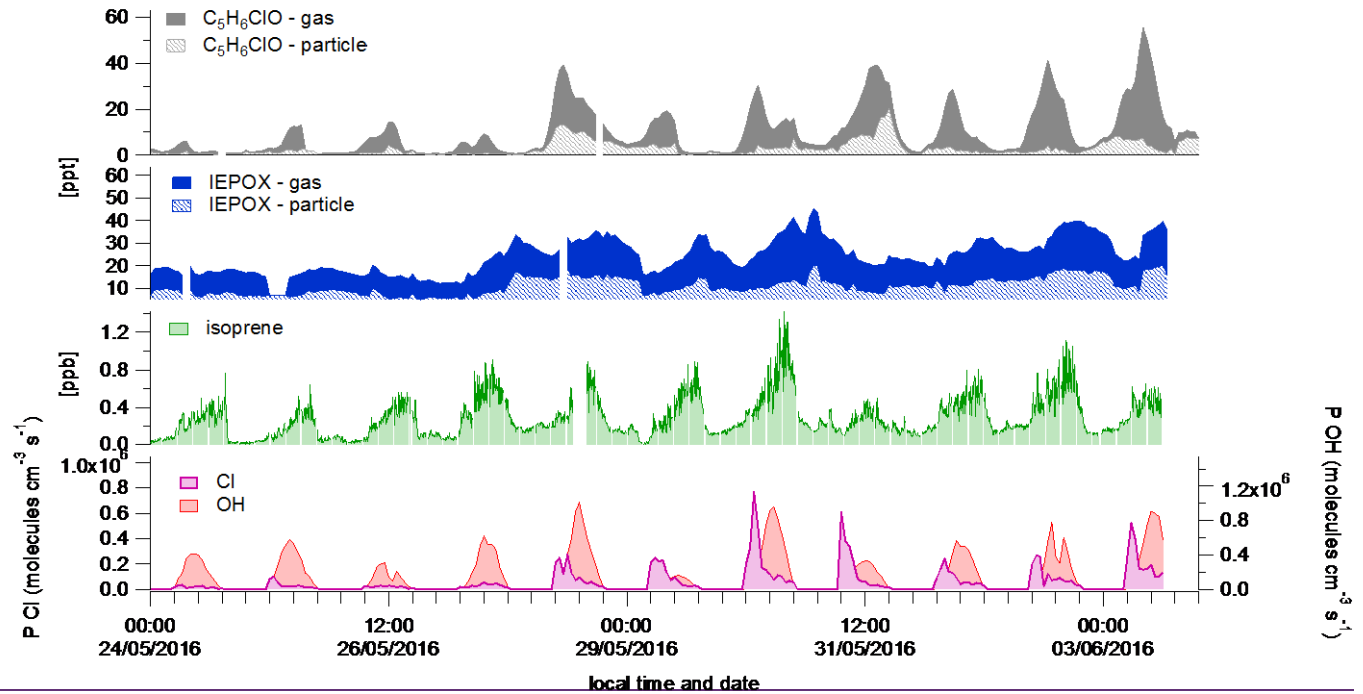
2 **Figure 7. A) Steady state calculation of inorganic halogens contribution to chlorine atom production. B)**
 3 **Relative mean diurnal profiles of calculated chlorine atom mixing ratio calculation from this work (Beijing)**
 4 **and measurements in the UK (London (Bannan et al., 2015) and a marine site (Weybourne Atmospheric**
 5 **Observatory-Bannan et al., (2017)). The steady state OH production rate from Beijing is also displayed to**
 6 **illustrate relative mixing ratios of oxidants.**



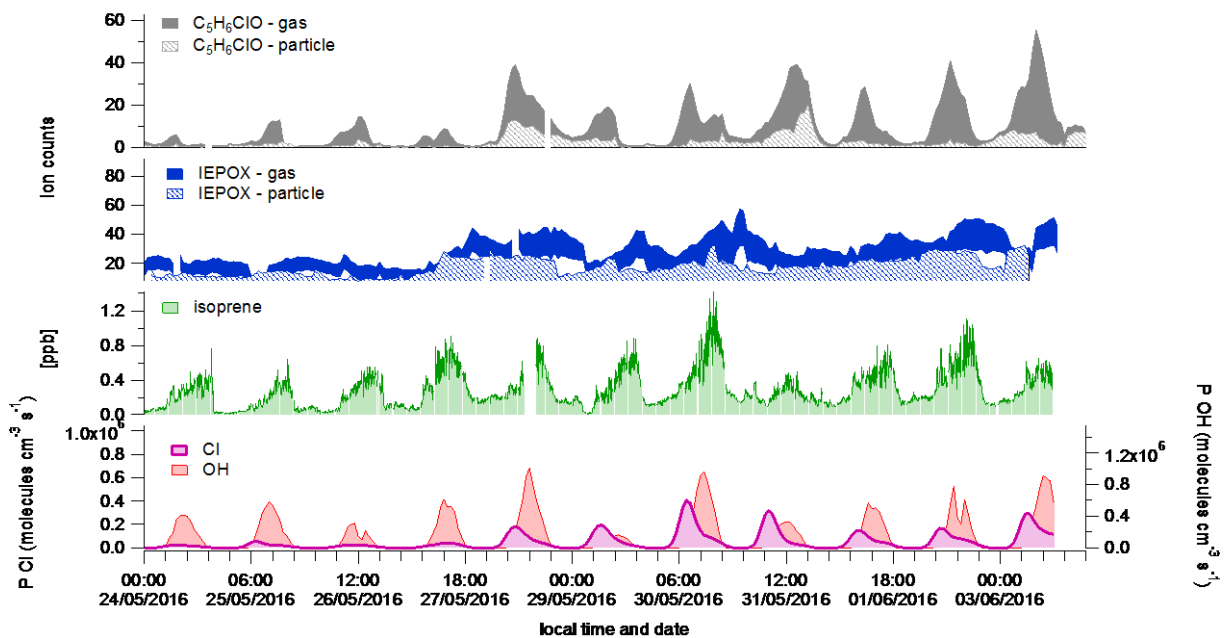
7

1 **Figure 8. Mean diurnal time series of alkene (pink) and alkane (blue) relative reaction rate (arbitrary value)**
 2 **with the chlorine atom (dashed) and OH (solid).**

3



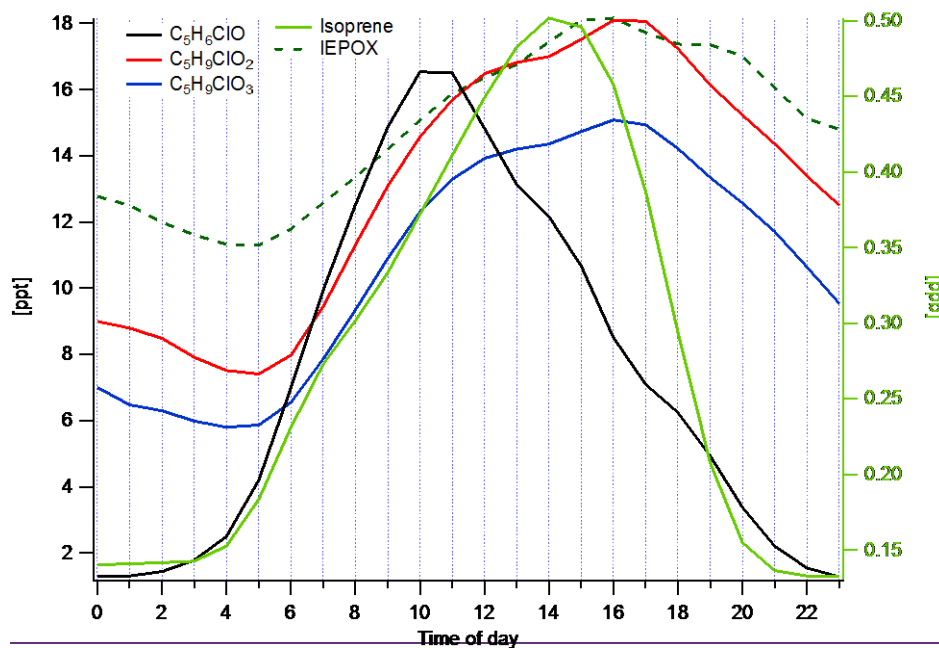
4



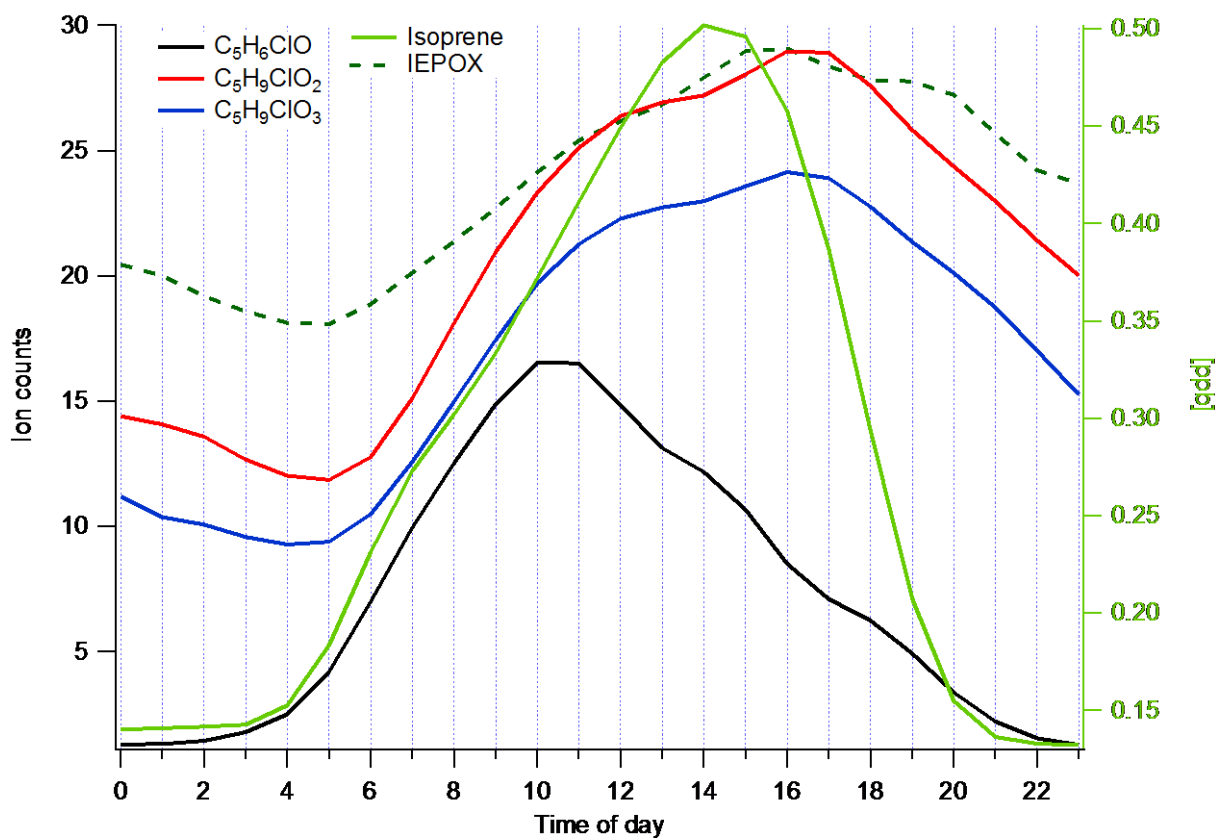
5

6 **Figure 9. Campaign time series of isoprene, IEPOX, CMBO and steady state production rate of chlorine**
 7 **atoms and OH**

8



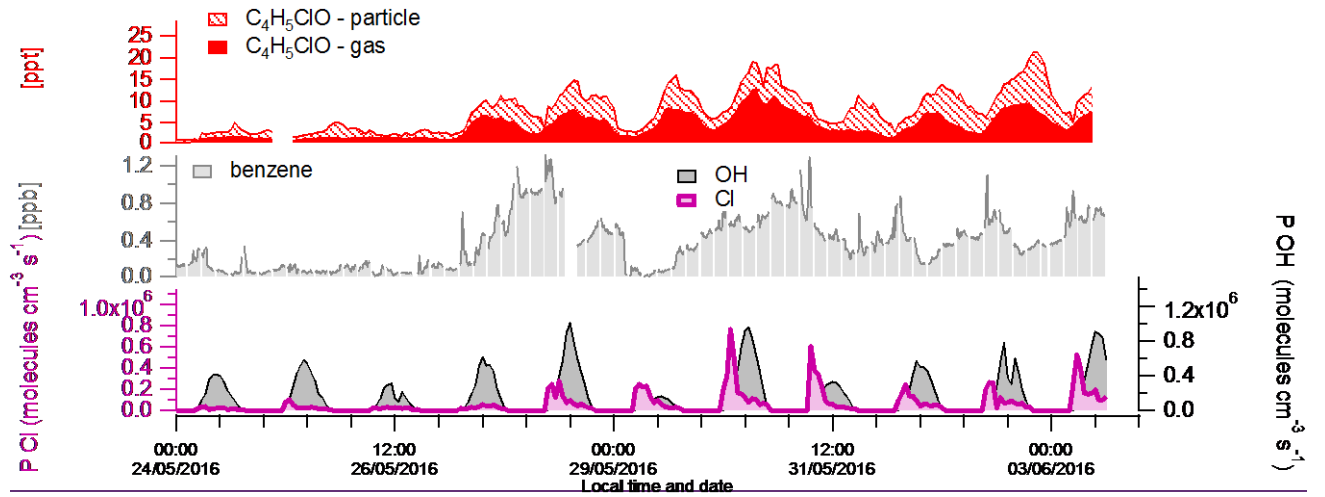
1



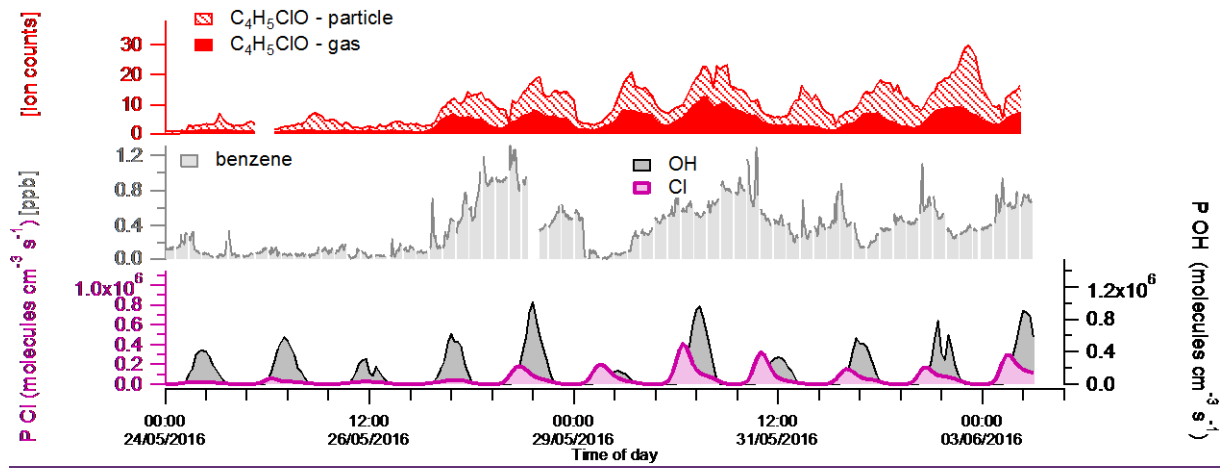
2

3 **Figure 10. Mean diurnal profiles of isoprene (right y-axis) and its OH oxidation product (IEPOX) and**
 4 **chlorine atom oxidation products CMBO, $C_5H_9ClO_2$ and $C_5H_9ClO_3$ (left y-axis)**

5



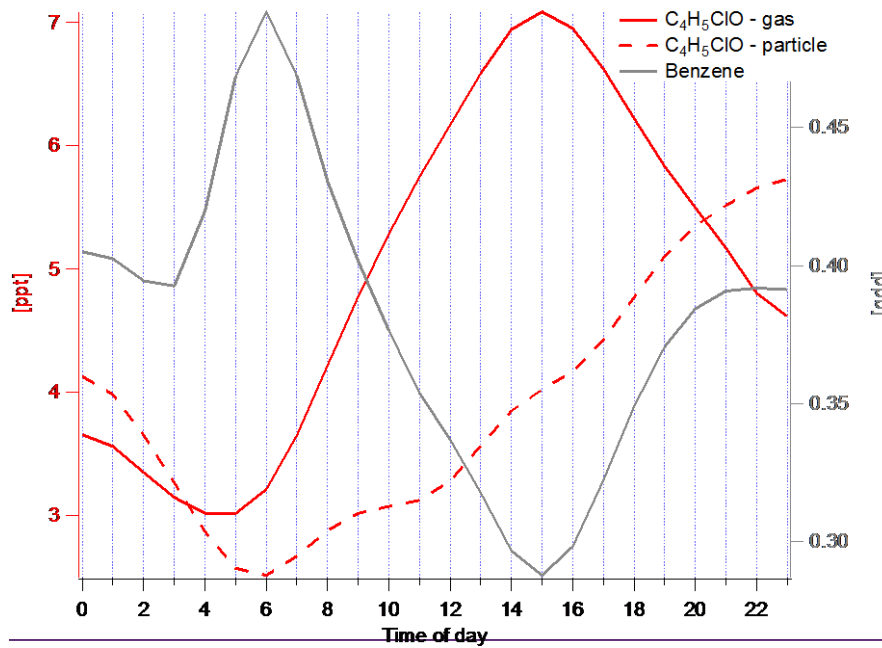
1



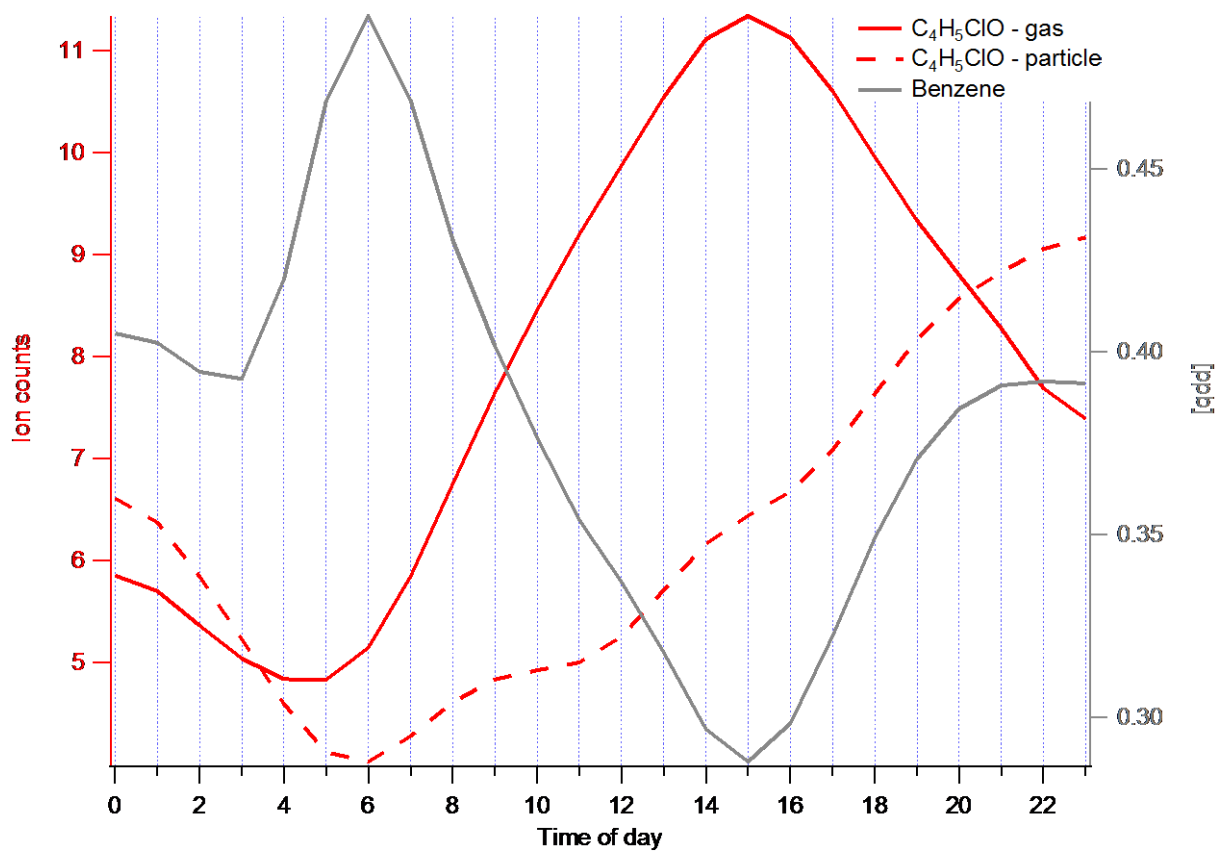
2

3 Figure 11. Campaign time series of benzene and CCA with supporting calculations of OH and
 4 the chlorine atom production rates

5



1



2

3 **Figure 12. Mean campaign diurnal profiles of benzene (grey) and CCA in the particle (dashed red) and gas**
 4 **phase (solid red).**

5